NTNU – Trondheim
Norwegian University of
Science and Technology

Modelling of Paraffin Wax in Oil Pipelines

Morten Kristoffer Siljuberg

Earth Sciences and Petroleum Engineering
Submission date: July 2012
Supervisor: Jon Steinar Gudmundsson, IPT

Norwegian University of Science and Technology
Department of Petroleum Engineering and Applied Geophysics

Abstract

As warm oil or condensate from the reservoir flow through a pipeline on the cold sea bottom, wax often precipitate and deposit on the wall. To predict the rate of the deposition, wax modeling is important. The main mechanism contributing to deposition, molecular diffusion, is driven by a radial concentration gradient. The concentration gradient is driven by the radial temperature gradient. When precipitation of wax crystallites occurs in the bulk of the flow, it affects the concentration gradient, which again affects the rate of deposition. The current thesis gives an elucidation of this particularity.

Fundamental heat and mass transport equations are solved numerically in Matlab and the result shows that the concentration profiles become slighter as the precipitation become larger. This decreases the mass flux due to molecular diffusion.

A term "shear dispersion" was introduced in 1980's to describe particle deposition of wax. The term has been used in several wax deposition models, but the mechanisms behind are not well explained in the literature. An elucidation of both a shear induced lift force and shear induced diffusion are investigated.

Preface

The work presented in this thesis is a result of the compulsory subject, TPG 4905 Petroleum production, master thesis. It was completed during the 10th semester of the Petroleum Engineering studies at NTNU. It was written at the Department of Petroleum Engineering and Applied Geophysics, spring 2012, and was delivered July 6th 2012. The work presented was conducted with Jon Steinar Gudmundsson as academic advisor.

I want to especially thank my advisor Jon Steinar Gudmundsson for introducing me to the interesting topic. I am grateful for all the inspiration and discussion throughout the work. I would also thank my fellow students for help and support during the semester.

Contents

List of Figures

List of Tables

Nomenclature

Latin symbols

ΔH_f	Heat of crystallization	J/kg
$\dot{m}$	Oil or condensate mass flow rate	kg/s
$\frac{dC}{dr}$	Concentration gradient	kg/m^4
$\frac{dT}{dr}$	Temperature gradient	K/m
ρ_n	Number density of nucleus	m/s
ρ_{gel}	Deposit's density	kg/m^3
A	Constant for the correlation of eddy viscosity	26
A_j^C	Coefficient for numerical concentration calculations	1/s
A_j^T	Coefficient for numerical temperature calculations	1/s
A_μ	Viscosity at a reference temperature	Pa $\cdot$ s
A_n	Nucleus surface	m^2
B_j^C	Coefficient for numerical concentration calculations	1/s
B_j^T	Coefficient for numerical temperature calculations	1/s
C	Wax concentration	[Kg/m^3]
C_j^C	Coefficient for numerical concentration calculations	1/s
C_j^T	Coefficient for numerical temperature calculations	1/s
C_b	Concentration of wax in the bulk	kg/m^3
C_p	Oil or condensate's spesific heat capacity	J/(K $\cdot$ kg)
C_s	Concentration of wax at the surface	kg/m^3
C_{wo}	Solubility of wax in oil	kg/m^3
D	Pipe's inner diameter	m
D_j^C	Coefficient for numerical concentration calculations	1/s
D_j^T	Coefficient for numerical temperature calculations	1/s
d_n	Nucleus diameter	m

D_{si}	Shear induced self diffusion coefficient	m^2/s
D_{wo}	Binary diffusion coefficient or mass diffusivity of wax in oil	m^2/s
E	Activation energy	J/mol
F_b	Force required to break the deposit	N
F_L	Actual lifting force due to shear	N
$F_{L(Saff)}$	Shear induced lifting force based on Saffmann's equation	N
h	Heat transfer coefficient	$W/(m^2 \cdot K)$
h_d	Mass transfer coefficient for a sphere	m/s
h_m	Mass transfer coefficient	m/s
J''	Mass flux	$kg/(s \cdot m^2)$
k	Constant for the correlation of eddy viscosity	0.4
k_f	Thermal conductivity	$W/(m \cdot K)$
k_r	Precipitation rate constant	1/s
$k_{r,cloud}$	Precipitation rate constant at cloud point	1/s
L	Distance from inlet	m
q''	Heat flux	$W/(m^2)$
r_i	The radial distance from pipe axis to the wall or liquid-deposit interface	m
r_p	Radius of suspended particle	m
T	Temperature	T°C
T_b	Temperature in the bulk	K
T_i	Pipe inlet temperature	K
T_s	Temperature at the surface	K
T_u	Ambient temperature	K
T_{cloud}	Cloud point temperature, equivalent with WAT	T°C
U	Overall heat transfer coefficient	$W/(m^2 \cdot K)$
u_τ	Friction velocity	m/s
V_z^+	Dimensionless turbulent velocity	–

V_a	Molar volume	m^3/mol
V_z	Axial velocity	m/s
y_z^+	Dimensionless distance from wall or wax-oil interface	–

Greek Symbols

α	Aspect ratio of wax crystallite	m/m
α_p	Volumetric fraction of suspended particles	m^3/m^3
α_T	Thermal diffusivity	m^2/s
β	Constant for heat of fusion for crystallization	–
δ_c	Concentration boundary layer thickness	m
δ_d	Deposits thickness	m
δ_t	Temperature boundary layer thickness	m
$\frac{dT}{dt}$	Cooling rate	F/min
$\dot{\gamma}$	Shear, or velocity gradient	1/s
μ	Oil or condensate's dynamic viscosity	$Pa \cdot s$
μ_a	Apparent viscosity	$Pa \cdot s$
ν	Kinematic viscosity of oil or condensate	m^2/s
ω	Solid wax content of a deposit	$weight - \%$
ϕ	Wax deposit porosity	$volume - \%$
ρ	Density of oil or condensate	kg/m^3
τ_w	Wall shear rate	Pa
τ_{gel}	Shear rate during formation of wax deposit	F/min
ε_h	Turbulent heat diffusivity	m^2/s
ε_m	Turbulent mass diffusivity	m^2/s
ε	Eddy diffusivity	$Pa \cdot s$
C_{bfc}	Breaking force coefficient	$weight - \%$

Dimensionless heat, mass and momentum transfer numbers

$Le = \frac{Sc}{Pr}$ Lewis number, represents the ratio between thermal diffusivity and mass diffusivity

$Nu = \frac{hD}{k_f}$ Nusselt number, represents the ratio between the heat transfer by conduction and the heat transfer by convection. Often referred to as the dimensionless convective heat transfer coefficient

$Pr = \frac{\nu}{\alpha_T}$ Prandtl number, represent the ratio of momentum diffusivity and thermal diffusivity

$Pr_T = \frac{\varepsilon}{\varepsilon_h}$ Turbulent Prandlt number

$Re = \frac{VD}{\nu}$ Reynolds number, represents the ratio between inertia and viscous forces, and are used to describe flow conditions

$Re_\gamma = \frac{\dot{\gamma} d_p^2}{\nu}$ Particle Reynolds number due to shear

$Re_s = \frac{V_s d_p}{\nu}$ Particle Reynolds number due to slip velocity

$Sc = \frac{\nu}{D_{wo}}$ Schmidt number, represents the ratio between momentum diffusivity and mass diffusivity

$Sc_T = \frac{\varepsilon}{\varepsilon_m}$ Turbulent Schmidt number

$Sh = \frac{h_m D}{D_{wo}}$ Sherwood number, represent the ratio between the mass transfer by conduction and the mass transfer by convection. Often referred to as the dimensionless convective mass transfer coefficient

---

Abbreviations

SPE Society of petroleum engineers

WAP Wax apperance point

WAT Wax apperance temperature. Equivalent to WAP and cloud point

1 Introduction

The worlds increasing thirst for oil, along with technological progress, has opened up for production and exploration in locations that earlier were not considered economically viable. The fields may be smaller and the environment may be colder and harsher. The use of subsea transportation of reservoir fluids has shown to be more efficient and because of colder environments and longer transport distances precipitation and deposition of solids in production and transportation equipment has become a bigger issue for the oil industry. In many deep-water fields, satisfactory subsea flow assurance is essential for a field's economic viability.

1.1 Crude composition

Crude oil consists of various chemical components: Paraffin, resins, bitumen, aromatics and naphthenes are some of the components that can be found[1]. Dependent on the amount of hydrogen available during maturation the hydrocarbons can be saturated or undersaturated. Saturated hydrocarbons are those where all the "spots" on the carbon atoms are taken by either a hydrogen atom or a neighbor carbon atom. Undersaturated are those where some of these bonds are double or even triple[2]. The former is known as paraffin and the latter can be naphthenes or aromatics, such as asphaltenes. Crude can either be paraffin-base or asphalt-base dependent on the major relative fraction of the former mentioned components.

The value of crude found in a reservoir is determined by how accessible the energy is. Hydrocarbons are usually sold to the end user as natural gas, gasoline, diesel or fuel oil. These products mainly consists of the smaller paraffins, ranging from C_1 up to C_{14}. Larger hydrocarbons need to be cracked in order to convert them into a saleable product, thus less profitable. In addition, they are often a bother for assured flow of oil and condensate from production site towards processing facilities and refineries. This is because these heavy molecules precipitate out of the oil or condensate due to reduction in pressure and temperature. These precipitates often deposit on production equipment such as flow lines and pipelines.

A typical method for determination of crude oil composition is by High Temperature Gas Chromatograph (HTGC). By evaporating the components in the oil or condensate, the vapor pressure of its respective components can be measured separately. The concentration of a compound is solely a function of its vapor pressure. A high temperature gas chromatogram for a wax-oil mixture is shown in Figure 1.1.

1.2 Wax as a flow assurance challenge

Among the components of crude, high molecular weight n-paraffins and asphaltenes are the notorious pipe cloggers; they are the cholesterol of the oil industry. A picture of a severe wax deposit is seen in Figure 1.2. In Figure 1.3 the precipitation line for three common solids in oil and gas industry is shown in a pressure temperature diagram. As seen here, the solubility line of wax is hardly a function of pressure, so wax deposition is considered to be only temperature dependent. Wax precipitate typically at lower temperatures than asphalthenes and are mainly

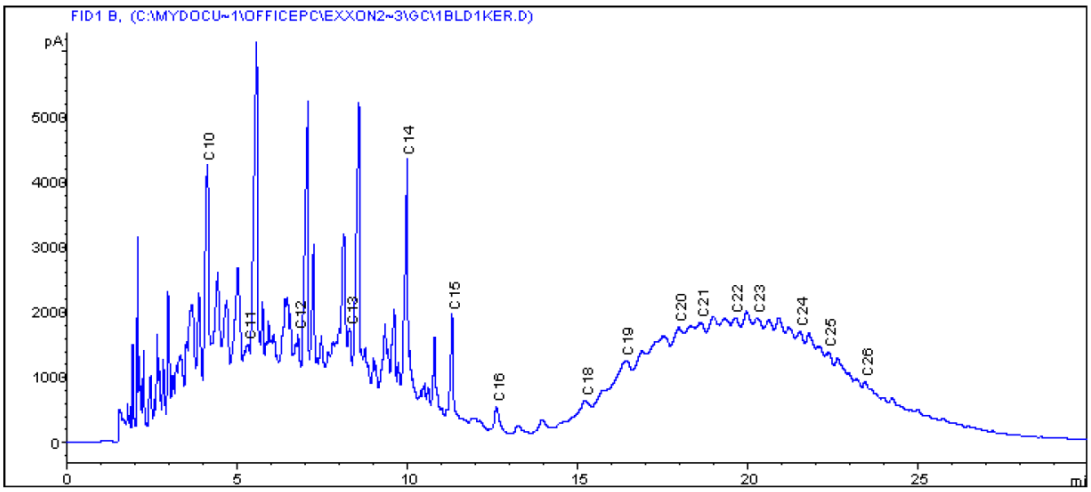

Figure 1.1: High temperature gas chromatogram for a wax-oil mixture used in flow loop experiments[1].

.

a problem in pipelines rather than flow lines, see Figure 1.4. Precipitation and deposition on pipeline wall due to temperature reduction in the pipeline, reduces the diameter available for flow and can even plug it completely.

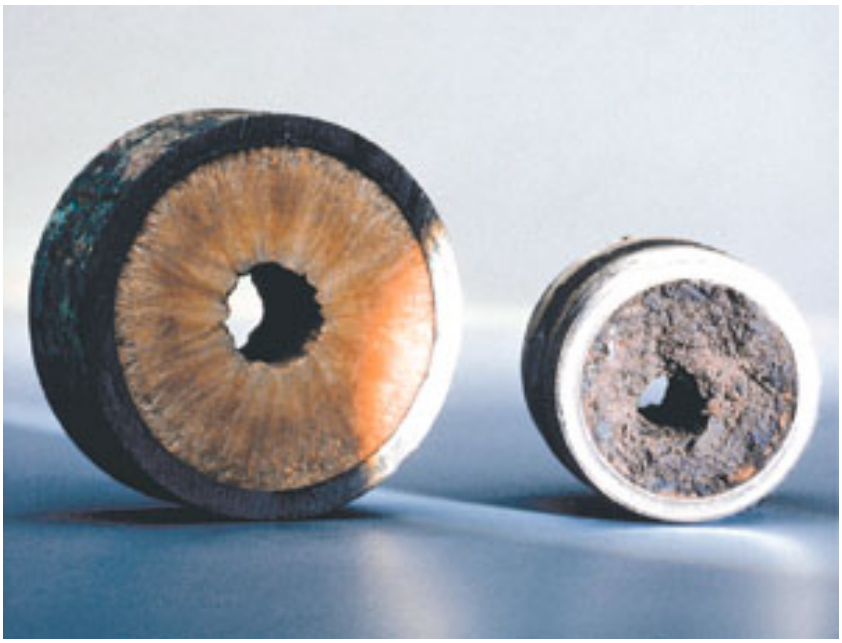

Figure 1.2: Pipeline segments with solid deposits. The left is a wax deposit and the right is a scale deposit[3].

Every once in a while production from a petroleum field need to be shut down. During the shutdown, wax is allowed to precipitate under static conditions. In these cases, wax deposition is not only limited to the wall, the whole bulk volume can stiffen into a gigantic wax-oil candle. When restarting the pipeline, a sufficiently high pressure is required to break the plug and make it flow again.

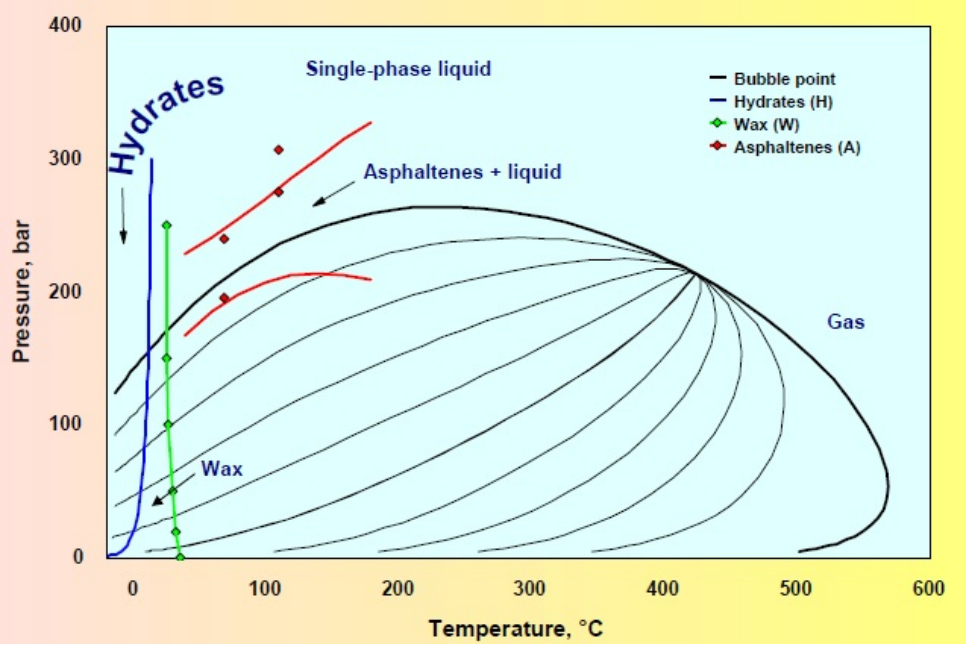

Figure 1.3: Typical pressures and temperatures for solid formation in petroleum production[4].

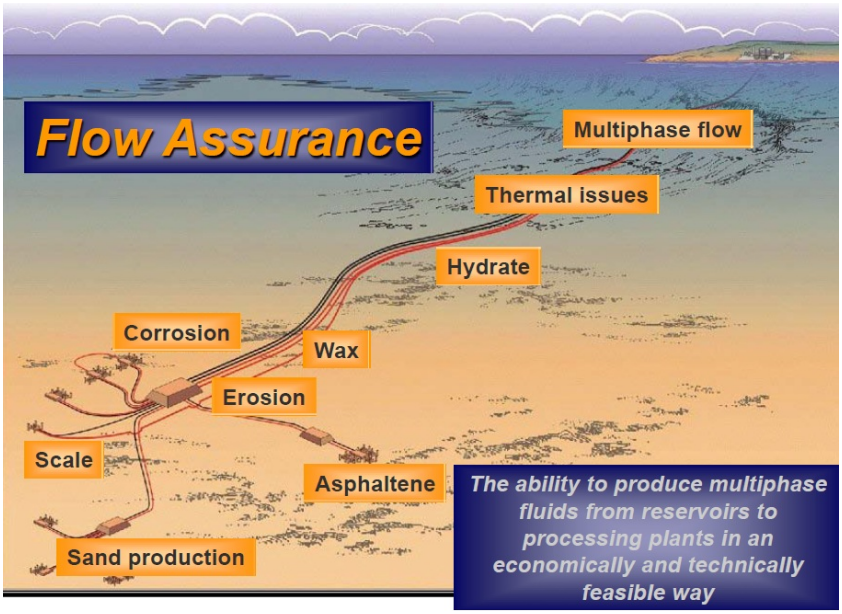

Figure 1.4: Typical flow assurance problems[5].

1.3 Solid management

If potential precipitates are present in a reservoir fluid, which often are, the developer must, during the planning of a field, find a economical suitable management for solid deposition. The management is dependent on the transportation length, surrounding water temperature, oil composition, et cetera. For a short pipeline or flow line the fluid temperature could be held sufficiently high by heating or insulating the pipe. For longer pipelines, heating or insulation becomes too costly. For such transportation lengths the fluid however reaches ambient temperature and all the potential solids will precipitate. However, insulation might also be used to evenly deploy the deposits over a larger distance of the pipeline, preventing large local build up, see Figure 1.5. In addition, it is shown by Venkatesan that a lower cooling rate makes the deposit softer, such that mechanical removal becomes easier[1]. This is elucidated in Chapter 9.

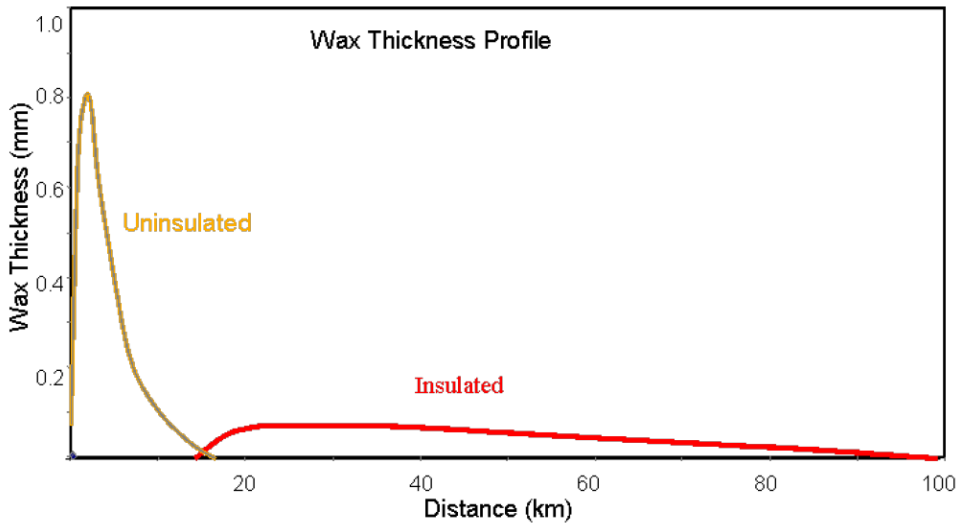

Figure 1.5: Difference in deposition profile between isolated and uninsulated pipeline[5].

A very common way to handle wax deposition in the industry today is by pigging. A pig is a tool that is sent through the pipeline in order to scrape away already deposited wax. The word pig comes from the scream-like sound it makes when it is sent through the pipeline. There are many types of pigs. Bypass, hard pigs, soft pigs, and more. All are suitable for different situations. Some for handling severe wax deposition problems and other used for regular cleaning/scraping of a pipeline. Since pigging is an expensive process, a thickness prediction as a function of time is essential in order to optimize the pigging frequency. The deposits strength is also an important factor here. Pigging requires back pressure to scrape away the wall deposit. As the deposit ages and becomes harder or bigger, the pressure requirement increases. This driving force comes either from the reservoir, or since a reservoir contains limited amount of pressure, a pump might be used.

Another way to handle wax deposition is the use of paraffin dispersant. By injecting such dispersant together with the oil, flocculation of wax is in some degree avoided. Small wax particles would flow toward the end of the pipe rather than depositing on the cold pipe wall. Though it is shown that the use of a paraffin dispersant in some cases can increase the rate of

paraffin deposition because the stability of colloidal asphaltenes are disturbed[6, 7].

A new non-conventional removal technique is frequent heating of the pipeline wall[8]. After a certain wax build up, the wax is removed by heating it from the inside. In this way, the wax near the wall liquefies and the forces holding the deposit to the wall are vanished. The deposit falls out in the stream and is transported towards the pipe outlet. By limiting the heating to only be powered for a short period of time, the expenses are dramatically reduced. See Figure 1.6 for illustration. The concept was patented in 2011[9].

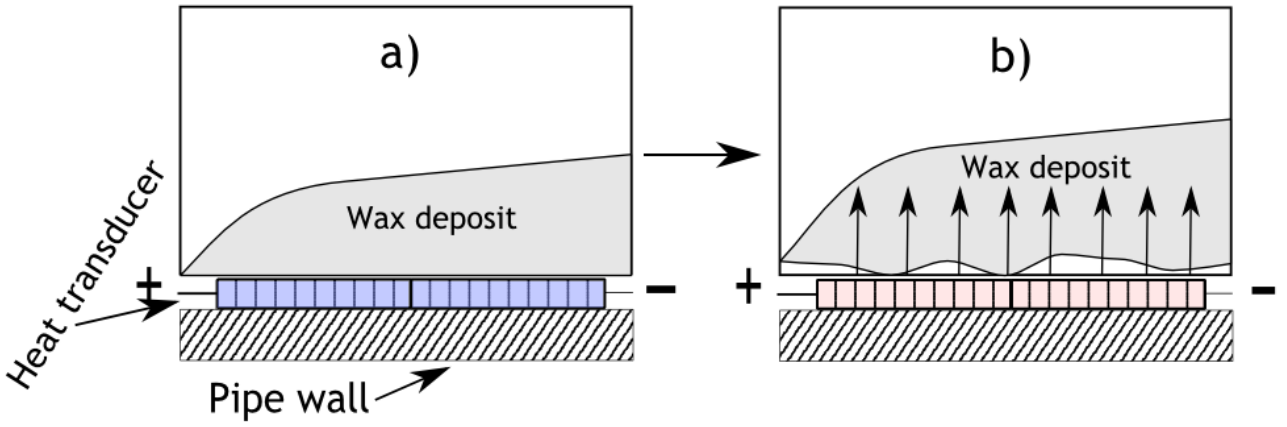

Figure 1.6: Wax removal with frequently heating.

Cold flow technology is a new prevention technique for solid deposition management[10, 11]. The technology focuses on transportation of hydrocarbons over long distances. After a cool down section the fluid is transported in thermodynamic equilibrium with the surroundings such that no further precipitation of solids is happening, see Figure 1.7. In this way, all the potential solids are precipitated out of solution in the cool down section and is transported together with reservoir fluids as a solid-liquid slurry. A crucial part of cold flow technology is that the precipitates solidified in the cool down section do not stick to the wall in the equilibrium section. The topic of particle deposition becomes relevant here, and one of the possible mechanisms is presented in Chapter 10.

To avoid solid deposition on the pipe walls in the cool down section, a solid repellent material to cover the inside of the pipeline walls would be perfect. Unfortunately, the researchers are struggling to find such a material. Until material scientists solve this puzzle, a remediation technique is needed for cold flow technology. Since the cool down section is small compared to the pipeline length, the remediation techniques become cheaper. In addition, it gives opportunities to new innovative, mechanically remediation techniques that would be applicable for shorter ranges. For example, a ferromagnetic scraper on the inside of the pipe wall could be driven by a electromagnet on the outside, see Figure 1.8. The Trondheim based company Empig AS was founded on such ideas and won both DNB's innovation contest and Adolf Øiens fund's establishment grant in 2011. The concept is patented[12].

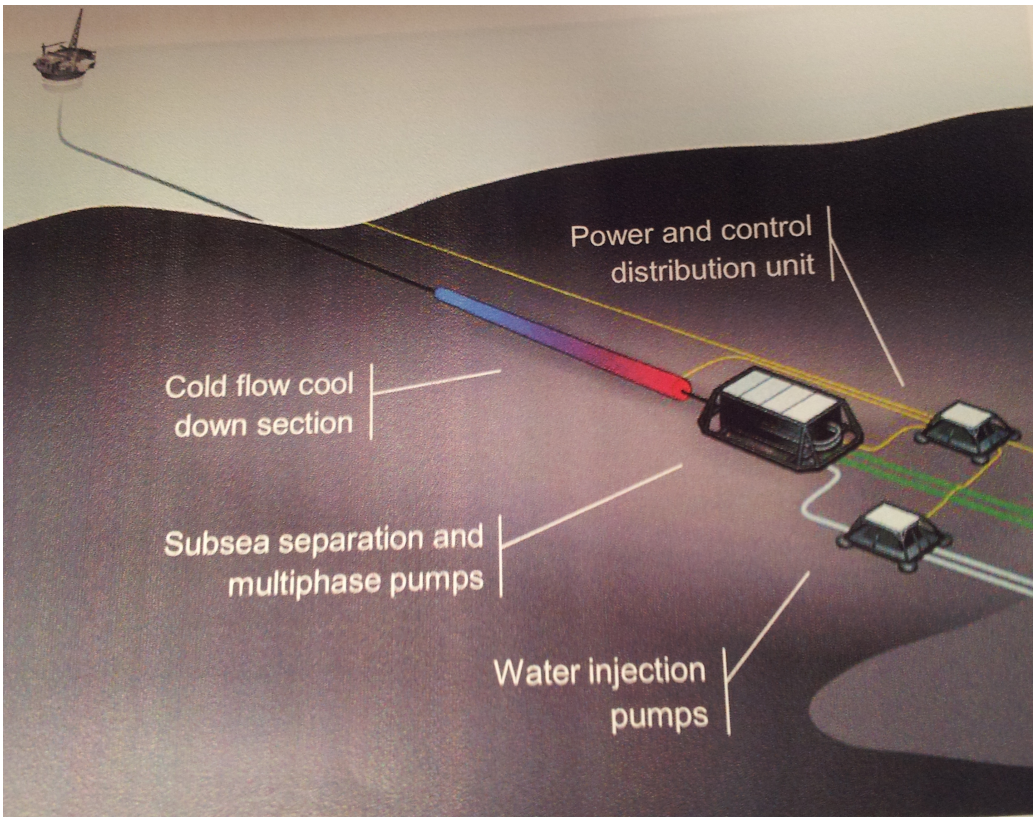

Figure 1.7: Cold flow concept[8].

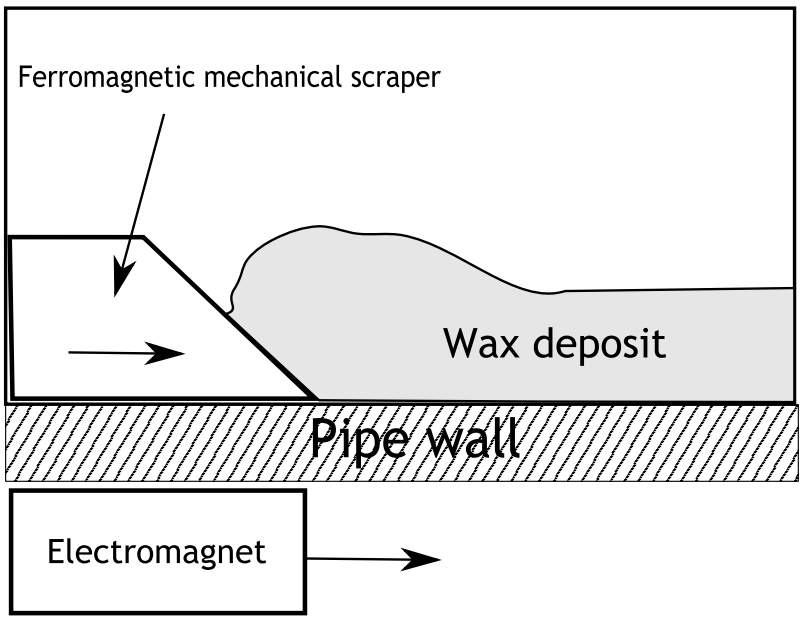

Figure 1.8: Mechanical removal of a wax deposit by a magnetic scraper.

1.4 Deposition rate quantification

Quantification of wax deposition severity is important in field development and design. Obviously, prediction of the deposits growth rate is important, but also its hardness plays a role. This is essential in planning the pigging frequency. After production start of a field, several measuring techniques can monitor the thickness profile of a solid deposit. Since solid deposition reduces the diameter available for flow, an increased fluid velocity causes a pressure reduction which can be used in deposit thickness estimation. An increased surface roughness may cause additional pressure drop that has to be considered.

Another method for deposit thickness determination is heat loss measurement at different points in the pipe. A given amount of heat is produced by a transducer, the heat spreads in 3 dimensions, and the deposit thickness can then be measured by the rate of heat loss. The conductivity of the deposit must be known. The thicker the deposits are, the slower will the temperature decrease. See Figure 1.9 for illustration. The method was patented by Amundsen and Hoffmann in 2011[9]

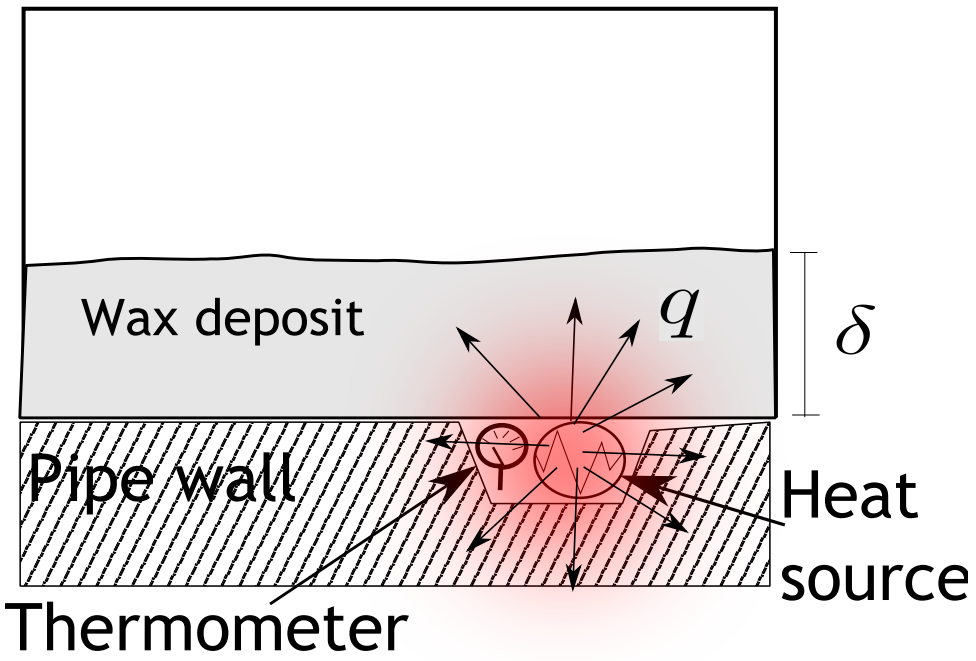

Figure 1.9: Measurement of deposit thickness by registering the temperature derivative.

Another method for determination of deposit thickness is the use of wax deposition models. By numerical calculation of the mechanisms causing deposition, one can forecast the rate of deposition along the pipeline. In the industry today, simulation software like OLGA is widely used for this purpose. Inputs and outputs of a typical wax deposition model is shown in Figure 1.10. Typical solubility curves of wax are shown in Figure 3.1. Since the deposition phenomena is quite complex, many of the existing models cannot accurately predict it, and they require empirical tuning parameters for correct prediction rate. It is also important to remember that a model, by definition, is wrong in some way.

The physical mechanism behind these deposition models vary from model to model and

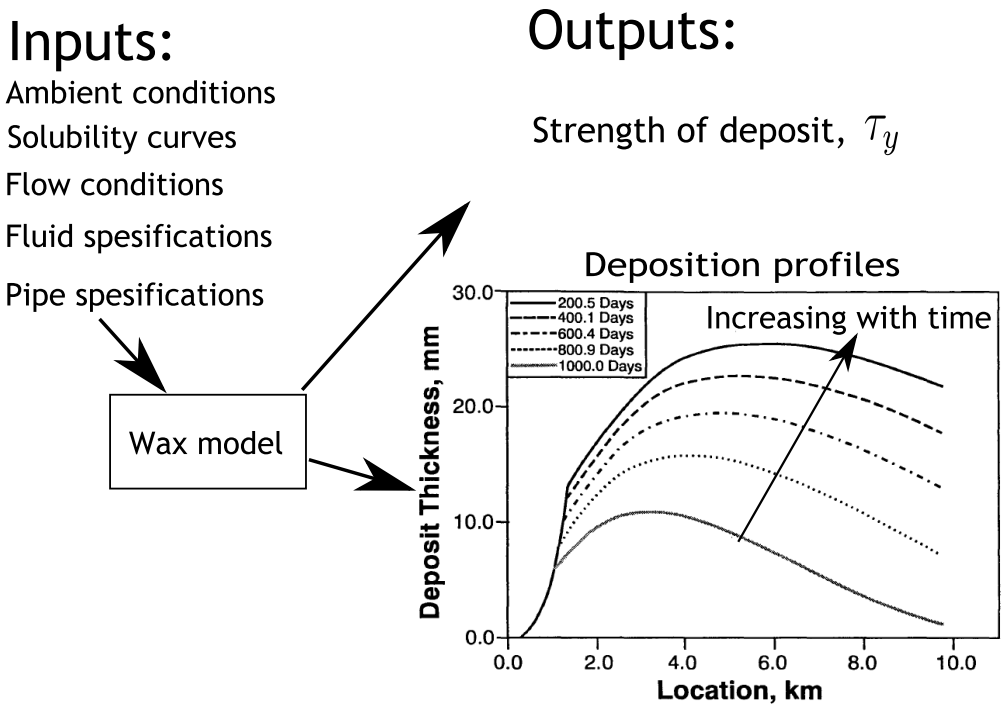

Figure 1.10: Basics of a deposition model.

vary in complexity. Different mechanisms have been suggested through the history: Molecular diffusion, soret diffusion, Brownian diffusion, particle agglomeration, gravity settling and shear dispersion[13, 14]. With the exception of molecular diffusion, all the above mentioned mechanisms are describing the radial transport of bulk precipitated particles. It is still discussed whether these particles deposit on the wall or continue along with the flow. Particle deposition mechanisms has been attempted disproved by many authors[13, 15, 16, 1]. Shear dispersion still remains questioned in the literature. Chapter 10 intends to elucidate the mechanisms behind the term.

After the wax is deposited on a pipeline wall it might also be removed as a result of the strong shear occurring in turbulent flows. The phenomena have several names in the literature, shear reduction, shear stripping and shear removal are some. Unfortunately the mechanism is difficult to describe analytically and little experimental data exist. But, empirical equations can be used to model the effects[17].

A further complexity for wax modeling is introduced when moving over to multiphase flow conditions. In the oil industry, transportation of gas and liquid are often transported in the flow lines or pipelines before separation. In a flow line, water produced from the reservoir might also be present. A study with numerical simulations of wax deposition in stratified flow was done by Huang et al[18].

An upper limit for deposition can be made from the solubility curve. Since the solubility of wax goes down with temperature it would tell us how much wax has precipitated out of the solution after a given temperature reduction. It does however not tell us anything about the growth of deposited wax on the wall, and should not be used for prediction of deposit thickness. It may be used in flow loop experiments and calculations where one is interested in

the volumetric fraction of solid wax particle in the bulk of the flow by subtracting the deposition rate.

During the last 10 years, a research group under the name "The University of Michigan Industrial Affiliates Program" has been developing a comprehensive wax model called "Michigan Wax Predictor". The model has a strong focus on the theoretical aspects behind the wax deposition processes. The program is sponsored with $45,000/year from some of the largest oil companies in the world, among others Statoil, ConocoPhillips and Schlumberger. Two PhD dissertations have been done, and the experimental results give valuable insight behind the mechanisms causing wax deposition. The current thesis is based largely on these two works[1, 19]. It is also important to mention that the current work is a continuation of the writers specialization project and specialization course autumn 2011[20, 21]. Some parts of the text written in the current thesis is taken from these work.

2 Transport phenomena

Transport phenomena is the study of how heat, mass and momentum is exchanged between systems. The latter is often difficult to grasp and we will not go into detail here. It is related to how fast the fluid velocity in decreases towards a stationary pipe wall. It is how the velocity profile develops. For further explanations we will focus on transport of heat and mass.

Transport phenomena is a wide discipline itself and since Bird et. al. wrote the first textbook on the subject in 1960[22], many others have been written on the same topic[23, 24, 25, 26]. For inexperienced, the theoretical concept might be difficult to understand. For further understanding the reader is referred to the books mentioned.

The reason for combining these phenomena in the same chapter is that heat and mass transfer can be described with equations of the same form. In heat and mass transfer we distinguish between advection and diffusion. Advection is bulk motion of fluid while diffusion is transfer of heat or chemical species within a fluid system. Convection is a term used to include the overall contribution of these two mechanisms together. In flow assurance context we are mostly concerned with fluid transportation through cylindrical tubes, such as flow lines or pipelines. Mass transfer can regard transport of wax molecules dissolved in the oil or tiny wax particles precipitated out of the solution.

In wax deposition theory we are mostly concerned with radial transport of wax towards the wall. But for crystal growth, mass transfer towards individual crystals is also relevant.

2.1 Heat and mass diffusion

Heat and mass diffusion, the former better known as conduction, is transport of heat and mass regardless of bulk fluid motion. The only driving force is the temperature or concentration differences. The heat and mass flux is described quantitatively as the temperature and concentration difference over a given interval of length, respectively.

$$q'' = -k_f \frac{dT}{dr} \tag{2.1}$$

$$J'' = -D_{wo} \frac{dC}{dr} \tag{2.2}$$

The former equation is known as Fourier's law and the latter as Fick's law. k_f is the oil or condensate's thermal conductivity. It must not be confused with α_T, which is the thermal diffusivity. D_{wo} is the binary diffusion coefficient of wax in oil. $\frac{dT}{dr}$ and $\frac{dC}{dr}$ is the temperature and concentration gradient, respectively. J'' represents the mass transfer per unit area, which is mass flux. q'' represents the heat transfer per unit area, that is heat flux. The reason we do not use the diffusivity in Fourier's law, is because temperature is not a transportable quantity, it is a state variable. Hence, we have to adjust it with the material's heat capacity and density: $k_f = \alpha_T \rho C_p$.

2.2 Turbulent pipe flow

Turbulent flow, which is often encountered in production technology, eddies and vortices complicate the transport phenomena. A turbulent eddy is a local swirling inside the bulk of the fluid; it is a chaotic advection. Mathematical description of these bulk motions are of great complexity, a simplification is therefore often used. Prandtl mixing length theory is a widely used simplification[27, p.227]. A mixing length, representing the length a fluid is transported due to an eddy is used to mathematically derive an eddy diffusivity equivalent to molecular diffusivity. In this way a superposition in Fourier's and Fick's includes heat and mass transfer contributions from both turbulence and diffusion in a similar manner[28, p 404, p. 467].

$$q'' = -(\alpha_T + \varepsilon_h)\frac{dT}{dr} \tag{2.3}$$

$$J'' = -(D_{wo} + \varepsilon_m)\frac{dC}{dr} \tag{2.4}$$

We have changed k_f with α_T to get consistency with the units of the eddy diffusivities. The mass and heat eddy diffusivities, ε_h and ε_m, are defined from Prandl mixing length theory as[28]:

$$\frac{\varepsilon_m}{D_{wo}} = \frac{Sc}{Sc_T}\frac{\varepsilon}{\nu} \tag{2.5}$$

$$\frac{\varepsilon_h}{\alpha_T} = \frac{Pr}{Pr_T}\frac{\varepsilon}{\nu} \tag{2.6}$$

Where Sc and Pr are the Schmidt's and Prandlt number, and Sc_T and Pr_T are their turbulent analogies, respectively. The numbers are explained in Chapter 2.4. ν is the kinematic viscosity of the oil or condensate. ε is the momentum diffusivity and is found from Van Driest's the following equation[29]:

$$\frac{\varepsilon}{\nu} = (ky^+)^2\left[1 - \exp\left(\frac{-y^+}{A}\right)\right]^2\left|\frac{dV_z^+}{dy^+}\right| \tag{2.7}$$

k and A are constants for the correlation of eddy viscosity and a value of 0.4 and 26 respectively suit this situation. y^+ and V_z^+ is the non-dimensional wall normal distance and velocity, normalized by u_τ. u_τ is the friction velocity and is defined by:

$$u_\tau = \sqrt{\frac{\tau_w}{\rho}} \tag{2.8}$$

Where τ_w is the wall shear stress and ρ is the fluids density. The dimensionless velocity is a function of its dimensionless distance from the wall in the following way:

$$V_z^+ = \begin{cases} y^+ & y^+ \leq 5 \\ 5\ln y^+ - 3.05 & 5 < y^+ < 30 \\ 2.5\ln y^+ + 5.5 & y^+ \geq 30 \end{cases} \tag{2.9}$$

where $y^+ = \frac{y}{\nu}\sqrt{\frac{\tau_w}{\rho}} = \left(1 - \frac{r}{R}\right)\frac{Re}{2}\sqrt{\frac{f}{8}}$, $f = \frac{0.305}{Re^{0.25}}$, $\kappa = 0.4$ and $A = 26$.

2.3 Convection

As stated earlier, convection is a term used to describe the collective contribution of advection and diffusion. This situation is more complex and the transport is calculated from Equation 5.1 and Equation 5.1 in Chapter 5. Most convective equations cannot be solved analytically, and we need numerical techniques to solve them, this is done in Chapter 5. Meanwhile, we introduce some easier equations that describes the transfer empirically:

For mass transfer:

$$J'' = h_m(C_b - C_s) \tag{2.10}$$

For heat transfer:

$$q'' = h(T_b - T_s) \tag{2.11}$$

T is temperature and C is concentration. Their subscripts s and b denotes the property at the surface and bulk average, respectively. h_m and h are the mass and heat transfer coefficients, respectively. The equations are known as Newton's law of cooling and is applicable for both mass and heat transfer. Finding the heat and mass transfer coefficient for specific cases are known as the problem of convection. The heat transfer coefficient can be found from the following equation:

$$h = \frac{-k_f \frac{\partial T}{\partial y}\Big|_{wall}}{T_s - T_b} \tag{2.12}$$

The mass transfer coefficient can be found from in similar manner:

$$h = \frac{-D_{wo} \frac{\partial C}{\partial y}\Big|_{wall}}{C_s - C_b} \tag{2.13}$$

2.4 Dimensionless numbers

To simplify the analysis, dimensionless numbers has been introduced for the convective heat and mass transfer equations. For heat and mass transport Nusselt and Sherwood number represent the dimensionless convective heat and mass transfer coefficients, respectively. The Nusselt number and the Sherwood number is is equated as follows[24]:

$$Nu = \frac{hD}{k_f} \tag{2.14}$$

$$Sh = \frac{h_m D}{D_{wo}} \tag{2.15}$$

By combining Equation 2.14 and Equation 2.15 with Equation 2.12 and Equation 2.13, respectively, the two following relationships are obtained:

$$Nu = \frac{-2r_i \frac{\partial T}{\partial r}|_{r=r_i}}{T_b - T_i} \tag{2.16}$$

$$Sh = \frac{-2r_i \frac{\partial C}{\partial r}|_{r=r_i}}{C_b - C_i} \tag{2.17}$$

r_i denotes the radial distance equal to the interface between either the oil and wall or oil and deposit. The Nusselt and Sherwood number is obtained by considering the temperature and concentration gradient at the wall, respectively. These two equations are later used in numerical simulations, see Chapter 6.

Two other important dimensionless quantities are the Schmidts and Prandtl number. The Schmidts number represents the ratio of momentum and mass diffusivity, and the Prandtl number is the ratio of momentum to heat diffusivity. They are defined as follows:

$$Pr = \frac{\nu}{\alpha_T} = \frac{C_p \mu}{k_f} \tag{2.18}$$

$$Sc = \frac{\nu}{D_{wo}} \tag{2.19}$$

In turbulent flow, there exists two analogous numbers:

$$Sc_T = \frac{\varepsilon}{\varepsilon_m} \tag{2.20}$$

$$Pr_T = \frac{\varepsilon}{\varepsilon_h} \tag{2.21}$$

They are called the turbulent Schmidt number and Prandlt number, respectively. The turbulent Prandtl number represents the ratio of turbulent mass diffusivity to the molecular mass diffusivity. The turbulent Schmidts number represents the ratio of thermal turbulent diffusivity to the molecular thermal diffusivity.

2.5 Convective boundary layers

Convective boundary layers are profiles that arise when a stream flows over a surface with a different temperature and concentration than in the flow. Incropera, P. and DeWitt, P. defines boundary layer as the distance from the wall where the temperature or concentration is 99% of the temperature or concentration in the free stream[24]. For internal cylindrical pipe flow we use the volumetric average over the bulk, T_b and C_b as the "free stream". The thickness of a temperature and concentration boundary layer is given by the symbol δ_t and δ_c, respectively. Figure 2.1 shows typical boundary layers for a flow over a flat plate. The study of boundary layers are important for a sufficient understanding of heat and mass transfer. The reader is here refered to literature on transport phenomena.

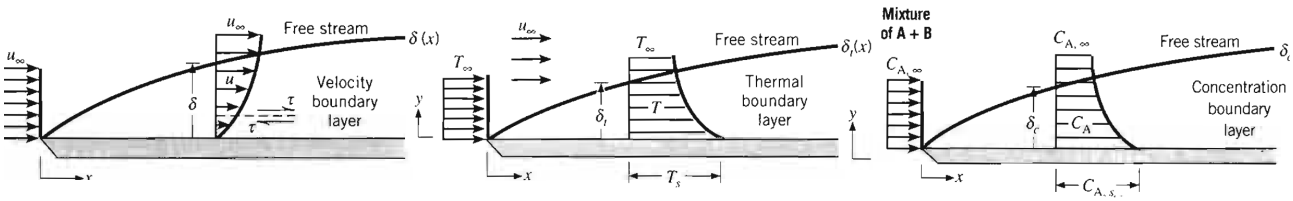

Figure 2.1: Velocity, temperature and concentration boundary layers for a stream flowing over a flat plate.[24]

2.6 Heat, mass and momentum correlations

As mentioned earlier, transport of heat, mass and momentum can be described with the same equations and are therefore said to be analogous. This is also reflected in the similarity of temperature, concentration and velocity profiles. Experimentally derived numerical correlations have been derived for the purpose of finding the convective heat and mass transfer equations.

For different geometries and flow conditions we have different correlations. We are mainly interested in correlations for turbulent, cylindrical pipe flow, but for the crystallization process of individual wax crystals a correlation for mass transport towards a spherical particle is also used. All the dimensionless numbers are declared in the nomenclature.

2.6.1 Turbulent pipe flow

For turbulent pipe flow, there has been developed several correlations for heat, mass and momentum transfer. One of these is the Dittus-Boelter correlation, which gives us the dimensionless convective heat transfer coefficient for a given Reynolds and Prandtl number:

For heat transfer:

$$Nu = 0.023 Re^{0.8} Pr^{0.3} \tag{2.22}$$

Equivalent for mass transfer:

$$Sh = 0.023 Re^{0.8} Sc^{0.3} \tag{2.23}$$

Other, more accurate correlations exists, but for simplicity Dittus-Boelter correlation is used. It should be commented that Equation 2.22 and Equation 2.23 only pertain for smooth pipes. The transfer rates become bigger with increasing roughness and the effect are discussed by Bhatti and Shah[30]. Wax deposition is known to have a more rougher surface than a bare steel pipe wall.

2.6.2 External spherical flow

A numerous heat and mass transfer correlations has been suggested for external spherical flow. Ranz and Marshall propose the following: [24, p. 415]:

$$Sh = 2 + 0.6 Re_s^{1/2} Sc^{1/3} \tag{2.24}$$

Where Re_s is the particle Reynolds number due to slip velocity and is defined as:

$$Re_s = \frac{(|V_f - V_p|d_p}{\nu} \tag{2.25}$$

Where d_p is the particle diameter, and V_p and V_f are the particle and fluid velocity, respectively. When the particles is moving with the same speed and direction as the surrounding fluid, the particle's Reynolds number is 0 and the Sherwood number for external spherical flow becomes 2. For particles of oblong nature, such as wax crystallites, the equation might need some adjustments.

3 Deposition by molecular diffusion

3.1 Solubility and WAT

An oil or condensate's ability to contain wax is called its wax solubility. Precipitation of wax particles happens due to a reduction in solubility. The solubility is a function of temperature and are decreasing with decreasing temperature. Plots of solubility versus temperature are widely used in the process of quantifying wax deposition. Typical solubility curves are shown in Figure 3.1. It should be mentioned that using the term solubility for this case is a simplification. Wax consists of a variety of higher alkanes. Each of these components has its own solidification temperature and do therefore not precipitate at the same temperature. As we see here, the solubility curves can be concave upwards or downwards. Its concavity depends on the oil or condensate's composition. It is important to point out the difference between concentration and solubility here. Concentration denotes the actual amount of wax present in the oil, while the solubility denotes the amount of wax that oil or condensate manages to contain.

When solubility of wax approaches the concentration of dissolved wax in the oil or condensate, the WAT is reached. WAT, or cloud point, is a term used in the petroleum industry to describe the temperature below which a "cloud" of wax crystals is visible to an optical detector, when cooling down a wax containing crude. The WAT is therefore a experimentally derived measure. In the current thesis the term WAT will be used to describe the thermodynamically solubility limit of wax in the oil or condensate, a theoretical measure.

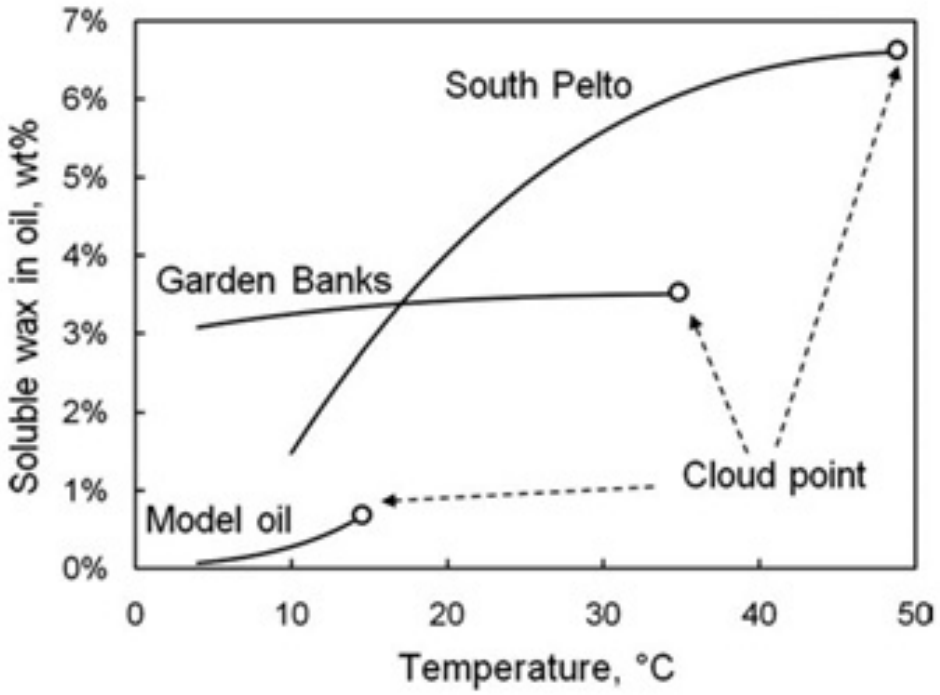

Figure 3.1: Solubility curves for different oils [31].

Data can also be given as wax precipitation curves. It is the opposite of solubility curve, and describes the amount of wax that precipitates as the temperature decreases. WAX modeling in AspenTech HYSYS requires this input rather than solubility, see Figure E.2.

3.2 Heat loss and wax crystallization

As the oil or condensate flow through the pipeline, its heat from the reservoir is gradually lost by heat transfer to the surroundings. This creates an axial temperature profile which is expressed by the following equation[32]:

$$T_L(L) = T_u + (T_i - T_u)exp\left(\frac{-U\pi D}{\dot{m}C_p}L\right) \tag{3.1}$$

T_u is the ambient temperature, T_i is the inlet temperature, U is the overall heat transfer coefficient, C_p is the oil or condensate's heat capacity and $\dot{m}$ is the mass flow rate in the pipe. T_L is the temperature of the flow at distance L from the inlet such that it is equal to T_m, which is the cross-sectional volumetric, temporal average of the flow[24, p.473].

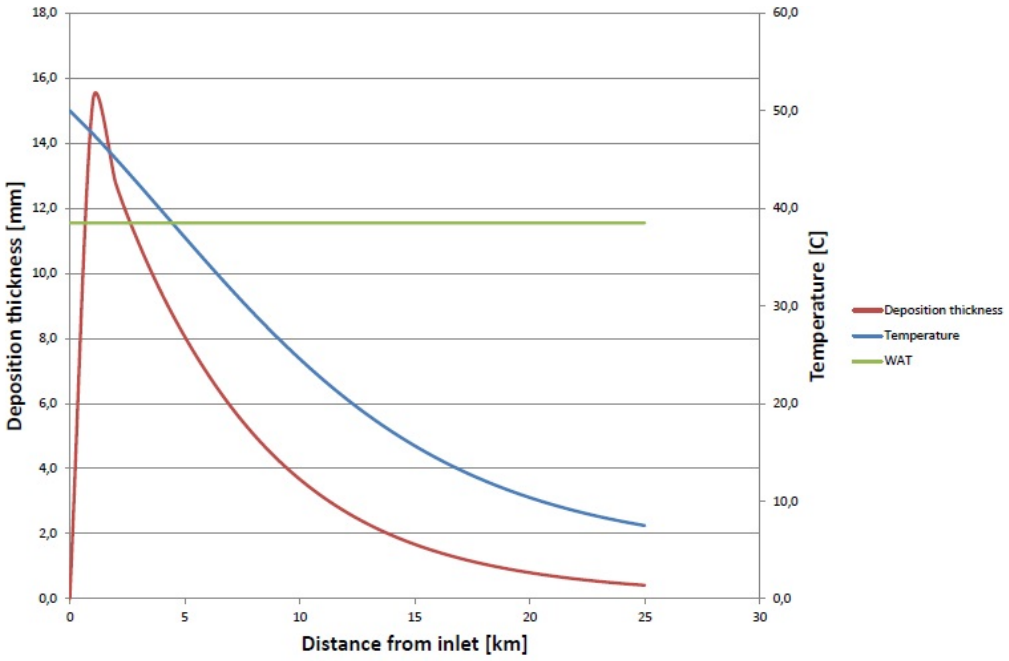

Figure 3.2: Temperature profile and deposit thickness.

In Figure 3.2 a typical temperature profile is illustrated together with deposition thickness. The simulations are done in HYSYS, and are explained in Appendix E. As seen from the figure, the deposition begins far before the WAT is reached. This is because the temperature in proximity to the wall reaches the WAT before the bulk average temperature does.

Inside the pipeline a temperature profile arise as a result of the heat loss to the environment. This temperature profile decides at which radial position the WAT is reached and thus where the wax crystallization may start, see Figure 3.3.

3.3 Temperature driven concentration profile

As the temperature near the wall decrease and wax precipitate out of the oil or condensate, the concentration of dissolved molecules decreases. This generates a driving force for molecular diffusion which again lead to a radial concentration profile in the pipe. Figure 3.4 show an

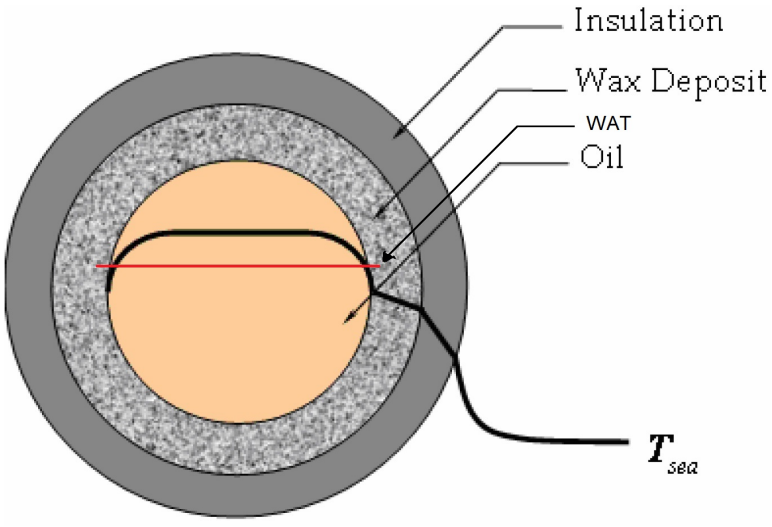

Figure 3.3: Illustration of radial temperature profile[1].

illustration of this. The picture can be a bit misleading; it is not necessarily the radial position of the WAT that decides the beginning of a decline in the concentration profile. If the WAT is located in immediate proximity to the wall or the wax-oil interface, precipitation and deposition of wax occurs only here. The concentration profile is then established exclusively as a result of this near-wall precipitation. This case was found to be true for laminar flow conditions[1].

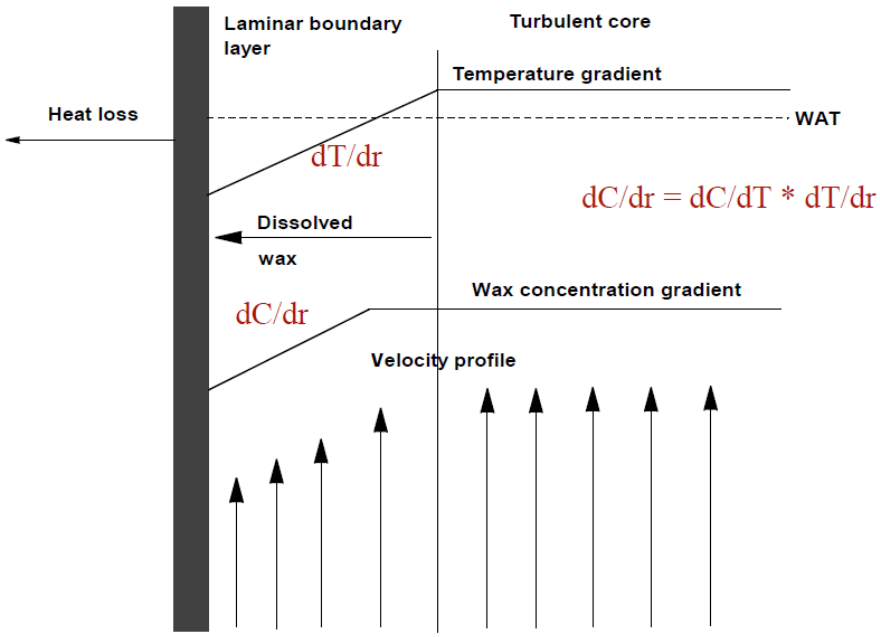

Figure 3.4: Temperature profile and its influence on concentration profile[33].

3.4 Impact of bulk precipitation

When precipitation of wax is allowed, not only in immediate proximity to the wall, but in the bulk of the flow, the concentration gradient becomes affected. How significant this effect is, is showed in Chapter 6. Let us call the distance from the wall or deposit where WAT is reached,

y_{WAT}. If $y_{WAT} > 0$, tiny wax crystallites are allowed to grow inside the bulk. Chapter 7 discusses some of the theory behind crystallization of these wax crystallites. In Figure 3.5, the green line represent the concentration of dissolved wax molecules as if we did not have bulk precipitation. When the red temperature profile deceeds[1] the solubility limit, WAT, the solubility profile does not follow the concentration gradient any longer and a supersaturation is arisen. The black line shows this solubility profile as a function of radial distance. It is determined from $\frac{dC_{wo}}{dr} = \frac{dT}{dr}\frac{dC_{wo}}{dT}$. From Equation 2.17, we see that a slighter concentration gradient at the wall causes less mass transport.

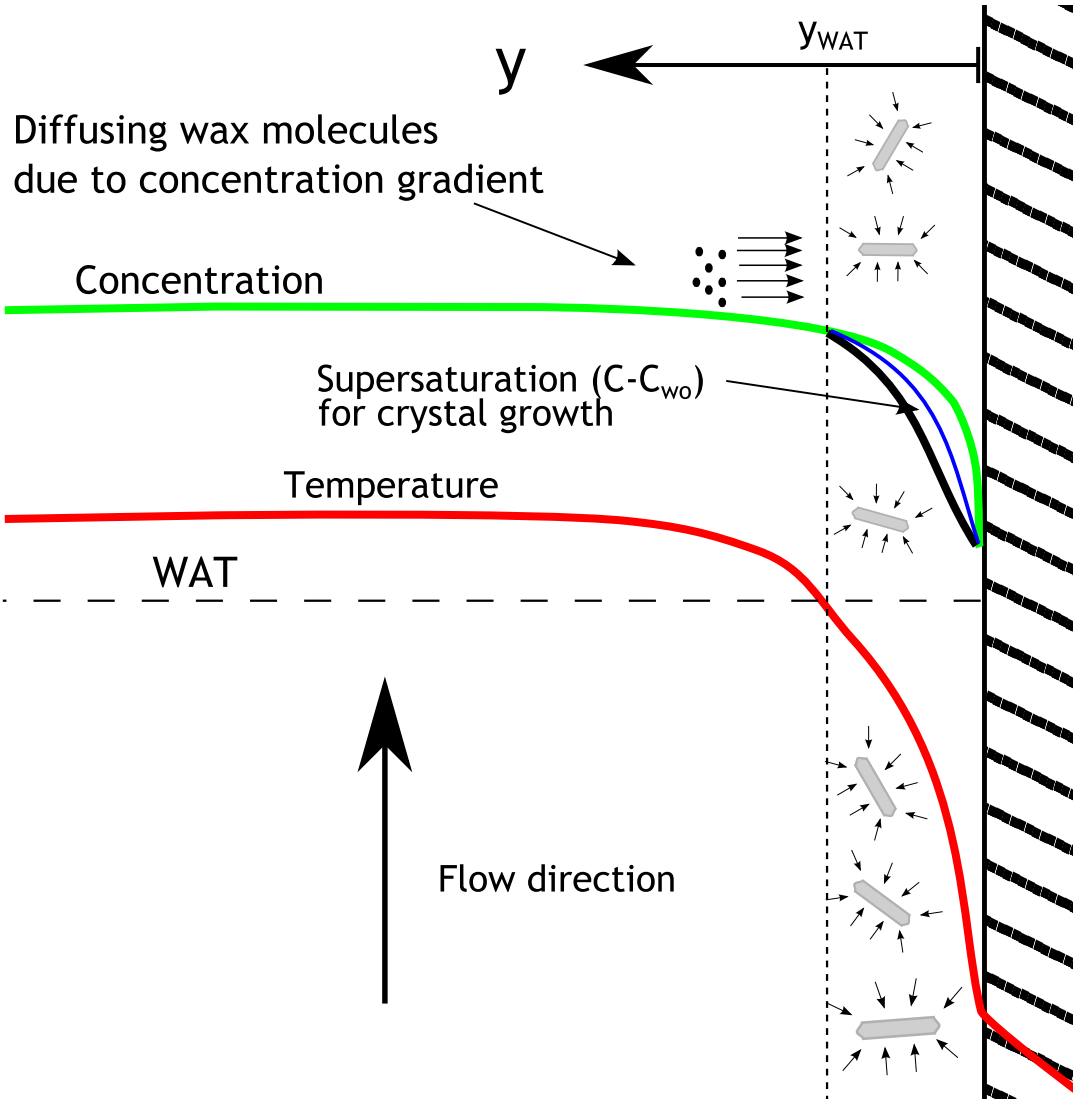

Figure 3.5: Illustration of how the concentration profile is affected by the temperature profile if WAT is located inside the flow.

For occasions where the concentration profile is affected by the temperature profile, ordinary heat and mass transfer analogies as described in Chapter 2.6 becomes unsuitable. These require boundary layer profiles established independently of bulk precipitation. The green line in Figure 3.5 shows how the concentration gradient would have been if bulk precipitation did

[1] An antonym of the word exceed is often needed. The word deceed has been suggested, but is still not accepted by Oxford dictionaries.

not occur. If bulk precipitation is present, the concentration gradient would exist somewhere in between the independently established concentration profile and the solubility profile. Where between the green and black line it will exist, depends on the rate that the wax crystallites precipitate. The precipitation rate is a function of the supersaturation multiplied with a precipitation rate constant.

$$G = k_r(C - C_{wo}) \tag{3.2}$$

Where C is the concentration at the position of interest and C_{wo} is the solubility of wax in the oil or condensate. k_r is the precipitation rate constant, and is discussed further in Chapter 4.4.

Singh et al. reports that bulk precipitation does not occur in laminar flow, it happens only when moving into the turbulent regime[19, 16, 1]. An explanation for this is though lacking in thepapers published from the University of Michigan.

3.4.1 Competing transfer rates

In order for the WAT to penetrate the bulk fluid, the "wax reservoir" in the bulk must not be depleted by molecular diffusion before the solubility approaches concentration, such that a supersaturation can arise. For this to happen, the heat transfer coefficient must be sufficiently large compared to the mass transfer coefficient. A too low heat transfer coefficient in laminar flow might be the reason that bulk precipitation is not observed here.

By plotting the Dittus Boelter correlations in Equation 2.22 and Equation 2.23 against the Reynolds number, we get an impression of how the heat and mass transfer rates increases compared to each other, see Figure 3.6. For our case, where the concentration gradient is dependent on the temperature profile, the relationship is actually a bit different, but the trends are similar. As we see, the heat transfer rate increases faster with increasing Reynolds number than the mass transfer rate.

If we include turbulent eddies into the considerations, the theoretical explanations increase in complexity. Increased turbulent mixing could increase the supersaturation for each crystallite, which in turn increases the crystallization rate. Precipitation rate of hydrates as a function of turbulent mixing is discussed in Marit Mork's PHD thesis[34].

Another approach to understand, is by comparing the size of the thermal and concentration boundary layers. The ratio between the thermal boundary layer thickness and the concentration boundary layer thickness is as follows[24, p. 354]:

$$\frac{\delta_t}{\delta_c} = Le^n = \frac{Sc}{Pr} = \frac{\alpha_T}{D_{wo}} \tag{3.3}$$

Where δ_t is the size of the thermal boundary layer and δ_c is the size of the concentration boundary layer. For most applications, $n = 1/3$. Typical for oils we have $Le >> 1$, see the values in Table 1. This indicates that heat is transfered faster than mass and the WAT can penetrate into the pipe. It should though be mentioned that the size of a boundary layer

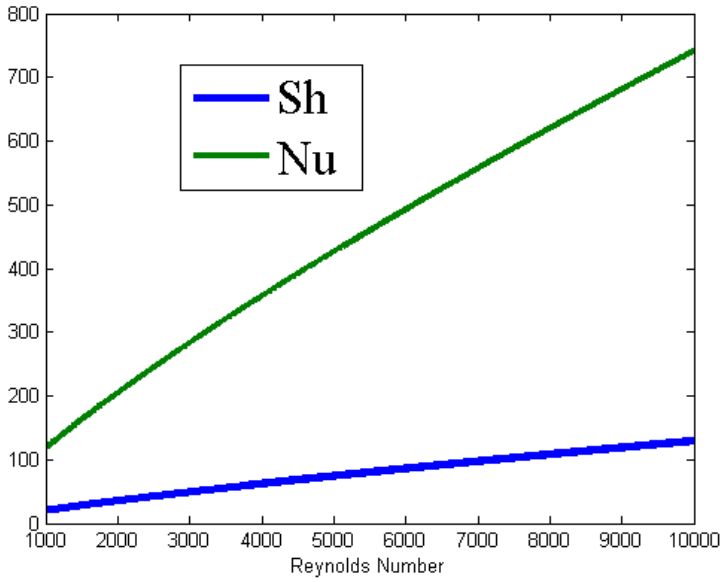

Figure 3.6: Sherwood versus Nusselt number from Diettus Boelter equation, Equation 2.22 and Equation 2.23. Pr=68 and Sc= 23.000 were used in the calculations, these are the numbers that Venkatesan reports for the wax-oil mixture in his experiments[35].

decreases with increasing flow rate[24]. This means for a higher flow rate, the penetration depth of y_{WAT} does not penetrate deeper in the pipe, just relative to the concentration boundary layer.

3.4.2 Discussion

In field development it is important to optimize the production of hydrocarbons and decrease the operating expenses. When a pigging solution is chosen as remediation technique, a lower frequency of pigging would be advantageous. If wax crystallites precipitated in the flow are not carried towards the wall and deposited here, an increase in the precipitation rate would be advantageous. This was also discussed in the writers previous specialization project[21]. To obtain this, it would be desirable to keep the WAT inside the bulk, such that a supersaturation is created for crystal growth. Thus, a high heat transfer coefficient relative to the mass transfer coefficient is needed, which is obtained by increasing the Reynolds number, see Figure 3.6. Experimental studies imply that a higher flow rates leads to slower growing deposit[1]. This is though usually explained with a shear removal mechanism that might occur in higher flow rates.

4 Quantifying molecular mass flux

In this chapter, 3 different methods for determination of the convective mass flux of wax molecules from bulk towards the wall are shown. All three methods involve finding the dimensionless convective mass transfer coefficient, Sh. The two first approaches use correlations from heat and mass transfer theory. In the third approach the Sherwood number is found by solving fundamental energy and mass conservation equations.

4.1 Independent heat and mass transfer method

Using heat and mass transfer analogy for wax deposition modeling was done by Singh et al[16]. A correlation that can be used is the Dittus-Boelter correlation, Equation 2.23. The method assumes that no wax molecules will precipitate in the bulk. Thus, all the wax molecules will deposit on the wall. It would result in an overestimation of the deposition rate. Consequently, the method calculates an upper limit for wax deposition due to molecular diffusion. It would be valid if $y_{WAT} = 0$.

4.2 Solubility method

In order to account for precipitation of wax in the bulk, a modification of the Dittus-Boelter correlation was done by Venkatesan[35]. An equation that accounted for the oils solubility was introduced. The following equation was proposed, which is derived in Appendix A.

$$Sh = Nu \frac{dC_{wo}}{dT} \frac{T_b - T_s}{C_b(T) - C_s(T)} \tag{4.1}$$

C_{wo} represents the solubility of wax in oil or condensate and is a function of temperature, C_b and C_s is the concentration of wax in the oil or condensate at their respective locations. Solubility curves as those shown in Figure 3.1 are used to obtain both the solubility gradient at the wall and the concentration at their respective places. The Nusselt number can be obtained from the Dittus-Boelter correlation since the temperature profile is independently established.

The solubility method assumes that wax will precipitate immediately as the solubility decreases. This is a simplification, since the crystallization process is not instantaneous. By overestimating the amount of precipitation in the bulk, the method underestimates the deposition rate by molecular diffusion. Hence, it represents a lower limit for the deposition rate due to molecular diffusion. Figure 4.1 illustrates how the Sherwood number is calculated as a function of the solubility curve.

4.3 Accounting for precipitation kinetics

Such as explained in Chapter 3.4, the inertia in the crystallization process of wax particles are needed to be accounted for in the determination of the mass flux by molecular diffusion. This is done by considering the kinetics of crystallization. The crystallization of wax molecules happen

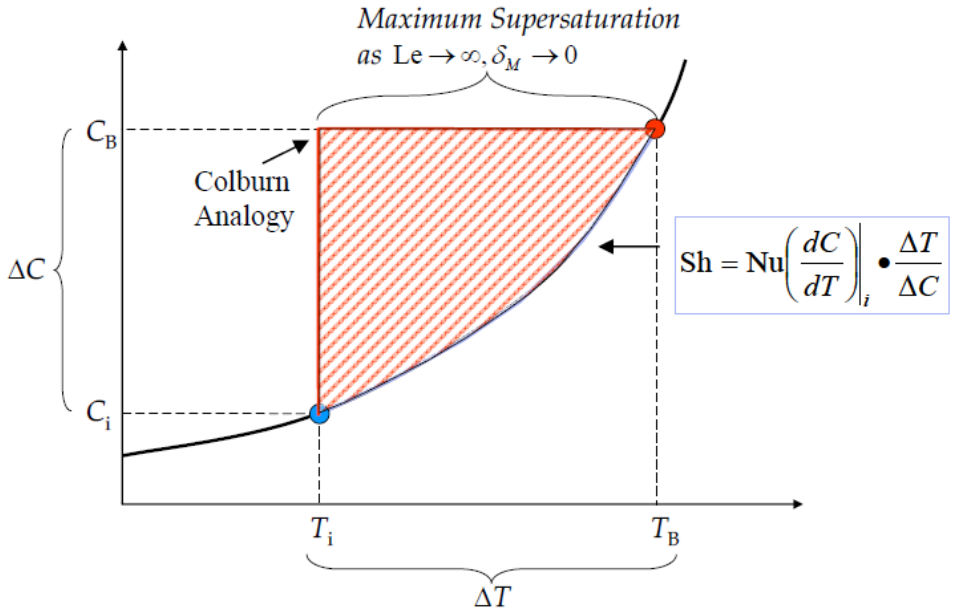

Figure 4.1: Illustration of how the Sherwood number is calculated by including the solubility of the oil or condensate. This is the solubility method[19].

because the solubility of wax in the oil deceeds the concentration the and a supersaturation is arisen. This supersaturation is determined by the difference between the solubility C_{wo} and concentration C. By including the kinetics, we cannot obtain a direct correlation for the Sherwood number, hence we need to solve fundamental heat and mass transfer equations. These equations are elucidated in Chapter 5.

For heat transfer:

$$V_z \frac{\partial T}{\partial z} = \frac{1}{r}\frac{\partial}{\partial r}\left[r(\varepsilon_h + \alpha_T)\frac{\partial T}{\partial r}\right] - \beta(C - C_{wo}) \tag{4.2}$$

For mass transfer:

$$V_z \frac{\partial C}{\partial z} = \frac{1}{r}\frac{\partial}{\partial r}\left[r(\varepsilon_m + D_{wo})\frac{\partial C}{\partial r}\right] - k_r(C - C_{wo}) \tag{4.3}$$

k_r is precipitation rate constant. The growths driving force is the supersaturation of dissolved wax molecules, $(C - C_{wo})$,

where

$$\beta \equiv \frac{k_r \Delta H_f}{\rho C_p} \tag{4.4}$$

ΔH_f is the heat of fusion, ρ is density and C_p is heat capacity.

The equations and a solution proposal is presented in Chapter 5.

4.4 Precipitation rate constant k_r

The precipitation rate constant k_r describes the crystallization speed quantitatively and is equated as[1]:

$$k_r = h_d A_n \rho_n \tag{4.5}$$

Where A_n is the surface of the nucleus, ρ_n is the number density of the nuclei and h_d is the mass transfer coefficient to the particles. h_d is found from the definition of the Sherwood number. If we assume spherical particles and that they are moving with approximately the same speed as the fluid surrounding them, that is particle Reynolds number close to zero, Equation 2.24 gives us 2. Together with the equation of the surface area of a sphere:

$$A_n = \pi d_n^2 \tag{4.6}$$

The precipitation rate constant becomes equated as:

$$k_r = 2\pi d_n \rho_n D_{wo}(T, \mu) \tag{4.7}$$

μ is the oil or condensate's dynamic viscosity and T is temperature. Obtaining a quantitative measure of d_n and ρ_n involves finding a solid-liquid thermodynamic equilibrium for the wax-oil system and is very complex. Hence, another approach is necessary to obtain a value of k_r.

k_r is a function of temperature and viscosity. Since viscosity is a function of temperature, k_r can be expressed as a function of just temperature. If k_r at a reference temperature is obtained we can use such a correlation to determine k_r at another temperature. Combinations of Equation B.2 and Equation C.2, described in Appendix B and Appendix C gives us a such correlation:

$$\frac{k_r}{k_{r,cloud}} = \left(\frac{T}{T_{cloud}}\right)^{1.47} exp\left(\frac{\gamma E}{R}\left(\frac{1}{T} - \frac{1}{T_{cloud}}\right)\right) \gamma = \frac{10.2}{V_a} - 0.791 \tag{4.9}$$

Here the cloud point is chosen as a reference temperature. V_a are molar volume. If we assume that $d_n$and ρ_n are independent of the radial distance this means that if we have the precipitation rate constant at a given temperature, we can obtain it at anywhere in the pipe.

5 Numerical solution of continuity equations

In physics, a continuity equation describes transport of a conserved quantity, such as energy or mass. Derivation of such equations are best understood by considering a finite control volume, as shown in Figure 5.1. Conservation of mass or energy is satisfied over the control volume. In radial coordinates the two conservation equations for mass and energy are:[36, 26].

For mass transfer:

$$\overbrace{\frac{\partial C}{\partial t}}^{Accumulation} + \overbrace{\left(V_r\frac{\partial C}{\partial r} + V_\theta\frac{1}{r}\frac{\partial C}{\partial \theta} + V_z\frac{\partial C}{\partial z}\right)}^{Advection} = \overbrace{(\varepsilon_m + D_{wo})\left[\frac{1}{r}\frac{\partial}{\partial r}\left(r\frac{\partial C}{\partial r}\right) + \frac{1}{r^2}\frac{\partial^2 C}{\partial \theta^2} + \frac{\partial^2 C}{\partial z^2}\right]}^{Diffusion} + \overbrace{R}^{Generation} \tag{5.1}$$

For heat transfer:

$$\overbrace{\frac{\partial T}{\partial t}}^{Accumulation} + \overbrace{\left(V_r\frac{\partial T}{\partial r} + V_\theta\frac{1}{r}\frac{\partial T}{\partial \theta} + V_z\frac{\partial T}{\partial z}\right)}^{Advection} = \overbrace{(\varepsilon_h + \alpha_T)\left[\frac{1}{r}\frac{\partial}{\partial r}\left(r\frac{\partial T}{\partial r}\right) + \frac{1}{r^2}\frac{\partial^2 T}{\partial \theta^2} + \frac{\partial^2 T}{\partial z^2}\right]}^{Conduction} + \overbrace{R}^{Generation} \tag{5.2}$$

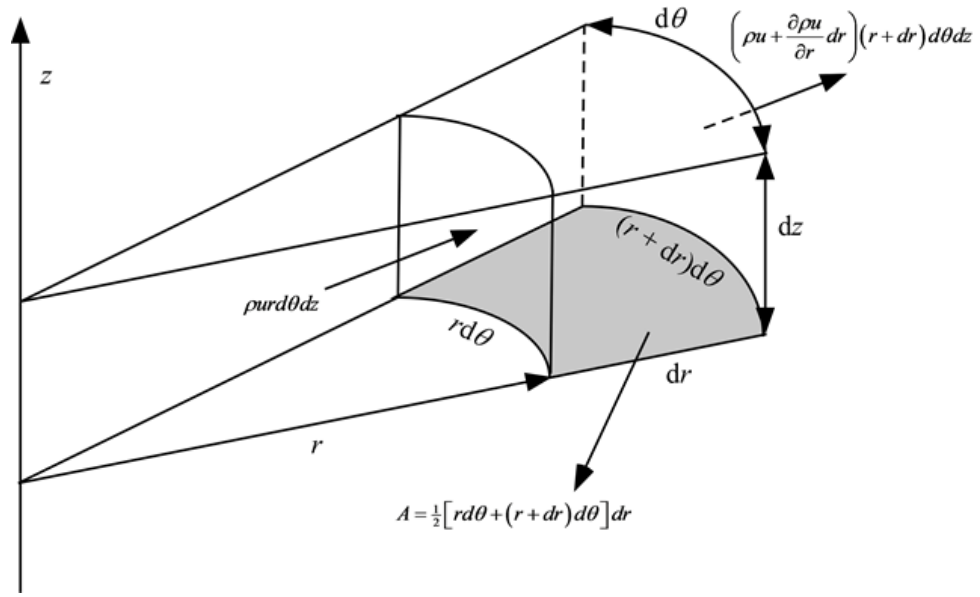

Figure 5.1: A cylindrical finite volume[37].

In turbulent pipe flow, eddies and vortices are causing local advection in all directions. As explained in Chapter 2.2, these small advective motions are summed up as diffusivity in direction of decreasing temperature of concentration. Advection is therefore only happening in axial direction. Diffusion in z-direction is very small compared to the transport caused by advection, so it can be neglected. The generation terms are sources or drains of mass or energy within a finite volume. We seek steady state solution, so the transient accumulation term is neglected. After removing the negligible parts of the equations we end up with the following equations for convection in turbulent pipe flow:

For mass transfer

$$V_z \frac{\partial C}{\partial z} = \frac{1}{r}\frac{\partial}{\partial r}\left[r(\varepsilon_m + D_{wo})\frac{\partial C}{\partial r}\right] - k_r(C - C_{wo}) \tag{5.3}$$

For heat transfer

$$V_z \frac{\partial T}{\partial z} = \frac{1}{r}\frac{\partial}{\partial r}\left[r(\varepsilon_h + \alpha_T)\frac{\partial T}{\partial r}\right] - \beta(T - T_{wo}) \tag{5.4}$$

The generation terms in the equations are caused by possible crystallization in the bulk of the flow. Mass is "lost" because of crystal growth and heat is gained from the crystallization process. Lee(2008) reports that heat of crystallization term are less than 0.1% compared to the advection and diffusion term, and can therefore be considered insignificant. The solution of these two equations is now shown separately in the two following chapters.

5.1 Heat transfer

Writing out the derivatives on the right hand side of Equation 5.4, neglecting the generation term and introduce a variable, α_{tot}, for the two terms, $\alpha_T + \varepsilon_h$, we get:

$$V_z \frac{\partial T}{\partial z} = \alpha_{tot}\frac{\partial^2 T}{\partial r^2} + \frac{\alpha_{tot}}{r}\frac{\partial T}{\partial r} \tag{5.5}$$

Discretization of the equation gives us:

$$v_z \frac{T_{i,j} - T_{i-1,j}}{\Delta z} = \alpha_{tot}\left(\frac{T_{i,j+1} - 2T_{i,j} + T_{i,j-1}}{\Delta r_j^2}\right) + \frac{\alpha_{tot}}{r_{j-1}}\left(\frac{T_{i,j+1} - T_{i,j}}{\Delta r_{j+1}}\right) \tag{5.6}$$

On the convection term on the right hand side, a backward difference discretization is used. On the second order radial diffusion term, a central difference discretization is used. On the first order diffusion term a forward difference discretization is used. Rearrangement of the temperature variables, we get it on the form:

$$A_j^T T_{i,j} + B_j^T T_{i,j+1} + C_j^T T_{i,j-1} = D_j^T \tag{5.7}$$

Where the coefficients are as follows:

$$A_j^T = \frac{v_{z,j}}{\Delta z_j} + \frac{1}{r_j}\frac{2}{\Delta r_{j+1} + \Delta r_j}\left\{\left[\frac{r_{j+1}\alpha_{tot,j+1} + r_j\alpha_{tot,j}}{2}\right]\left(\frac{1}{\Delta r_{j+1}}\right) + \left[\frac{r_j\alpha_{tot,j} + r_{j-1}\alpha_{tot,j-1}}{2}\right]\left(\frac{1}{\Delta r_j}\right)\right\} \tag{5.8}$$

$$B_j^T = -\frac{1}{r_j}\frac{2}{\Delta r_{j+1} + \Delta r_j}\left\{\left[\frac{r_{j+1}\alpha_{tot,j+1} + r_j\alpha_{tot,j}}{2}\right]\left(\frac{1}{\Delta r_{j+1}}\right)\right\} \tag{5.9}$$

$$C_j^T = -\frac{1}{r_j}\frac{2}{\Delta r_{j+1} + \Delta r_j}\left\{\left[\frac{r_j\alpha_{tot,j} + r_{j-1}\alpha_{tot,j-1}}{2}\right]\left(\frac{1}{\Delta r_j}\right)\right\} \tag{5.10}$$

$$D_j^T = \frac{v_z T_{i-1,j}}{\Delta z} \tag{5.11}$$

An elaborated description of the equation can be found in [27]. The grid can be viewed in Figure 5.2.

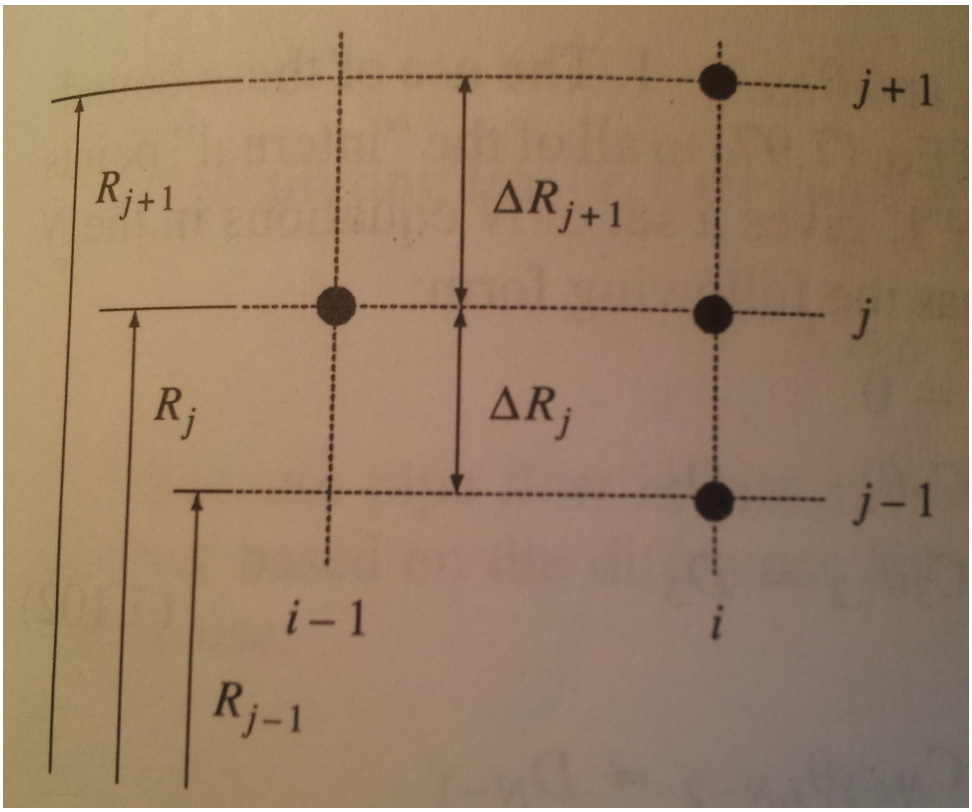

Figure 5.2: Grid structure.

For a uniform grid, it means that the differentials are equal over the whole grid, $\Delta r_i = \Delta r_{i+1}$), the coefficients will reduce to:

$$A_j^T = \frac{v_{z,j}}{\Delta z_j} + \frac{1}{2r_j \Delta r^2}(2r_j \alpha_{tot,j} + r_{j+1}\alpha_{tot,j+1} + r_{j-1}\alpha_{tot,j-1}) \tag{5.12}$$

$$B_j^T = -\frac{1}{2r_j \Delta r^2}(r_{j+1}\alpha_{tot,j+1} + r_j \alpha_{tot,j}) \tag{5.13}$$

$$C_j^T = -\frac{1}{2r_j \Delta r^2}(r_j \alpha_{tot,j} + r_{j-1}\alpha_{tot,j-1}) \tag{5.14}$$

For laminar flow, that means that the diffusivity is equal to the thermal diffusivity, α_T throughout the radius, the coefficients reduces further down to:

$$A_j^T = \frac{v_z}{\Delta z} + \frac{2r\alpha_T}{\Delta r^2} \tag{5.15}$$

$$B_j^T = -\frac{\alpha_T}{\Delta r^2} \tag{5.16}$$

$$C_j^T = -\frac{\alpha_T}{\Delta r^2} \tag{5.17}$$

D_j^T remains the same for all cases. The final linear system looks like:

$$\begin{pmatrix} 1 & -1 & 0 & 0 & 0 & \cdots & 0 & 0 & 0 \\ C_2 & A_2 & B_2 & 0 & 0 & \cdots & 0 & 0 & 0 \\ 0 & C_2 & A_2 & B_2 & 0 & \cdots & 0 & 0 & 0 \\ 0 & 0 & C_2 & A_2 & B_2 & \cdots & 0 & 0 & 0 \\ \vdots & \vdots & \vdots & \vdots & \vdots & \ddots & \vdots & \vdots & \vdots \\ 0 & 0 & 0 & 0 & 0 & \cdots & C_{N-1} & A_{N-1} & B_{N-1} \\ 0 & 0 & 0 & 0 & 0 & \cdots & 0 & 0 & 1 \end{pmatrix} \begin{pmatrix} T_{i,1} \\ T_{i,2} \\ T_{i,3} \\ T_{i,4} \\ \vdots \\ T_{i,N-1} \\ T_{i,N} \end{pmatrix} = \begin{pmatrix} D_1 \\ D_2 \\ D_3 \\ D_4 \\ \vdots \\ D_{i,N-1} \\ T_{wall} \end{pmatrix}$$

To obtain all the temperatures in our 2-dimensional grid, the system is solved semi-iterative. This means we use matrix calculation to solve implicit for all T's in radial direction, while we solve explicit in the axial direction. That means that we are solving implicit for all T's in radial direction, with matrix calculation, and explicit in the axial direction. The linear system in radial direction depends on the previous values in axial direction. This is reflected in vector D_j^T. An illustration is shown in Figure 5.3. All the disks are a function on the previous disk. The first disk is the inlet temperature to the pipe. How to make the coefficient matrix and solve the linear system is showed in Matlab script 1 and Matlab script 2.

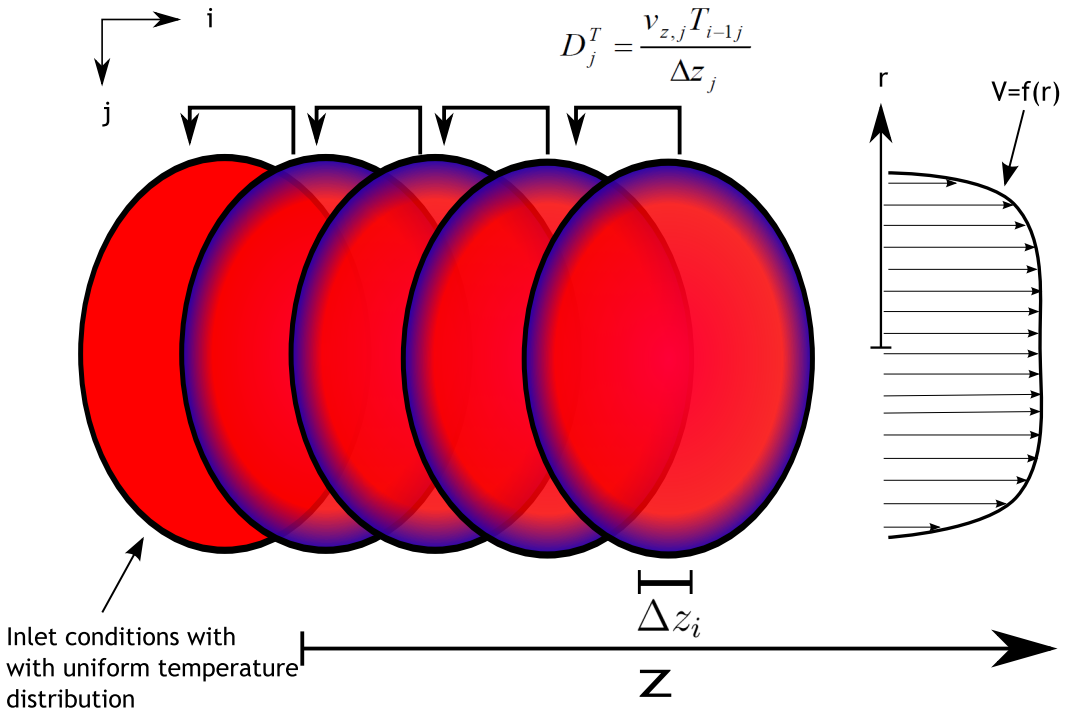

Figure 5.3: Illustration of the semi-iterative matrix calculation.

5.2 Mass transfer

The same procedure follows for the mass transfer equation.

$$V_z \frac{\partial T}{\partial z} = D_{wo,tot} \frac{\partial^2 T}{\partial r^2} + \frac{D_{wo,tot}}{r} \frac{\partial T}{\partial r} + k_r \tag{5.18}$$

Where $D_{wo,tot} = D_{wo} + \varepsilon_m$. The same discretization done for heat transfer equation can be done for mass transfer:

$$v_z \frac{C_{i,j} - C_{i-1,j}}{\Delta z} = D_{wo,tot} \left(\frac{C_{i,j+1} - 2C_{i,j} + C_{i,j-1}}{\Delta r_j} \right) + \frac{D_{wo,tot}}{r_{j-1}} \left(\frac{C_{i,j+1} - C_{i,j}}{\Delta r_{j+1}} \right) + k_r \tag{5.19}$$

Rearrangement of the concentration variables gives us:

$$A_j C_{i,j} + B_j C_{i,j+1} + C_j C_{i,j-1} = D_j \tag{5.20}$$

With the coefficients:

$$A_j^C = \frac{v_{z,j}}{\Delta z_j} + \frac{1}{r_j} \frac{2}{\Delta r_{j+1} + \Delta r_j} \left\{ \left[\frac{r_{j+1} D_{wo,tot,j+1} + r_j D_{wo,tot,j}}{2} \right] \left(\frac{1}{\Delta r_{j+1}} \right) + \left[\frac{r_j D_{wo,tot,j} + r_{j-1} D_{wo,tot,j-1}}{2} \right] \left(\frac{1}{\Delta r_j} \right) \right\} + k_r \tag{5.21}$$

$$B_j^C = -\frac{1}{r_j} \frac{2}{\Delta r_{j+1} + \Delta r_j} \left\{ \left[\frac{r_{j+1} D_{wo,tot,j+1} + r_j D_{wo,tot,j}}{2} \right] \left(\frac{1}{\Delta r_{j+1}} \right) \right\} \tag{5.22}$$

$$C_j^C = -\frac{1}{r_j} \frac{2}{\Delta r_{j+1} + \Delta r_j} \left\{ \left[\frac{r_j D_{wo,tot,j} + r_{j-1} D_{wo,tot,j-1}}{2} \right] \left(\frac{1}{\Delta r_j} \right) \right\} \tag{5.23}$$

$$D_j = \frac{v_z C_{i-1,j}}{\Delta z} \tag{5.24}$$

For a uniform grid, the equations reduce to:

$$A_j^C = \frac{v_{z,j}}{\Delta z_j} + \frac{1}{2 r_j \Delta r^2} (2 r_j D_{wo,tot,j} + r_{j+1} D_{wo,tot,j+1} + r_{j-1} D_{wo,tot,j-1}) \tag{5.25}$$

$$B_j^C = -\frac{1}{2 r_j \Delta r^2} (r_{j+1} D_{wo,tot,j+1} + r_j D_{wo,tot,j}) \tag{5.26}$$

$$C_j^C = -\frac{1}{2 r_j \Delta r^2} (r_j D_{wo,tot,j} + r_{j-1} D_{wo,tot,j-1}) \tag{5.27}$$

For laminar flow, that means that the diffusivity is equal to the diffusion coefficient, D_{wo}, throughout the radius, the coefficients reduce further down to:

$$A_j^C = \frac{v_z}{\Delta z} + \frac{2 r D_{wo}}{\Delta r^2} \tag{5.28}$$

$$B_j^C = -\frac{D_{wo}}{\Delta r^2} \tag{5.29}$$

$$C_j^C = -\frac{D_{wo}}{\Delta r^2} \tag{5.30}$$

Our linear system looks like:

$$\begin{pmatrix} 1 & -1 & 0 & 0 & 0 & \cdots & 0 & 0 & 0 \\ C_2 & A_2 & B_2 & 0 & 0 & \cdots & 0 & 0 & 0 \\ 0 & C_2 & A_2 & B_2 & 0 & \cdots & 0 & 0 & 0 \\ 0 & 0 & C_2 & A_2 & B_2 & \cdots & 0 & 0 & 0 \\ \vdots & \vdots & \vdots & \vdots & \vdots & \ddots & \vdots & \vdots & \vdots \\ 0 & 0 & 0 & 0 & 0 & \cdots & C_{N-1} & A_{N-1} & B_{N-1} \\ 0 & 0 & 0 & 0 & 0 & \cdots & 0 & 0 & 1 \end{pmatrix} \begin{pmatrix} C_{i,1} \\ C_{i,2} \\ C_{i,3} \\ C_{i,4} \\ \vdots \\ C_{i,N-1} \\ C_{i,N} \end{pmatrix} = \begin{pmatrix} D_1 \\ D_2 \\ D_3 \\ D_4 \\ \vdots \\ D_{i,N-1} \\ C_{wo}(T_{interface}) \end{pmatrix}$$

6 Simulations

In Appendix F an overview of all the functions needed to do simulations are described. Matlab script 6 shows how the functions are used to produce the figures in the current thesis.

6.1 Solving the linear system implicit

How to produce and solve the linear systems derived in Chapter 5 is shown in Matlab script 1 and Matlab script 2. The concentration matrix is more computational expensive than the temperature matrix. This is because the coefficient matrix needs to be reproduced for each axial step. An increment in data points in axial direction increase the simulation time proportional to ni. In radial direction, an increase of nj increases the size of the matrix such that the simulation time increases at a much faster rate. How much faster is determined by the algorithm Matlab uses to solve it.

6.2 Including turbulent diffusivities

To produce the coefficient matrices in Matlab script 2 and Matlab script 1 we need to obtain the diffusivities as a function of radial distance. As mentioned, the coefficient matrix for the concentration matrix does also depend on the axial distance. For turbulent flow conditions, the magnitude of turbulent eddies decreases as we approach the wall. The diffusivities are therefore varying with radial distance. α_{tot} and $D_{wo,tot}$ are as mentioned a sum of the molecular diffusivities and the turbulent diffusivities, such as explained in Chapter 2.2. The equations become: $\alpha_{tot} = (\alpha_T + \varepsilon_h(r))$ and $D_{wo,tot} = (D_{wo} + \varepsilon_m(r))$. At the bottom of Matlab script 2 and Matlab script 1 there is implemented two subfunctions which calculate the total diffusivities at a given radial distance. Both depends on the eddy diffusivity, whose function is implemented in Matlab script 4. Matlab script 3 describes a function returning the solubility of the oil of interest. For this work, a solubility curve for Norne Crude was used.

Variable	Value	Units
μ	4	cp
ρ	900	kg/m^3
α_T	$9.8 \cdot 10^{-7}$	m^2/s
ν	$4.44 \cdot 10^{-6}$	m^2/s
T_w	7	C°
T_i	70	C°
R	0.00794	m
Q	0.00063	m^3/s
V_a	435	cm^3/mol

Table 1: Simulation inputs. Heat and mass transfer values are taken from [1].

6.3 Simulation results

The completion and implementation of the model was too time consuming and a full implementation of the wax deposition model was not attainable. The intention with the simulations is to reproduce similar figures and plots that are found in Lee's PHD- thesis [19]. The figures show qualitative consistency; this indicate a correct code implementation. The data used for input to the model is shown in Table 1.

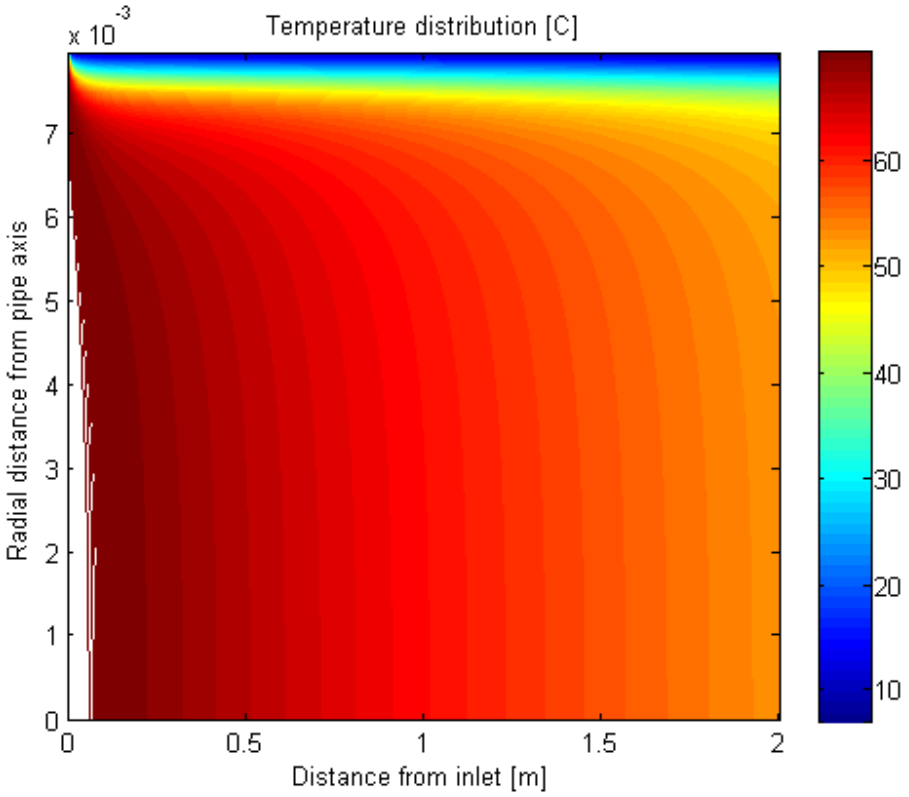

Figure 6.1: A contour plot of the temperature distribution in the pipe. The colorbar represents the oil's temperature in $°C$.

Figure 6.1 shows a 2-dimensional contour plot of the temperature grid produced in Matlab script 2. The colorbar on the left hand side represent the temperature in Celsius.

Figure 6.2 shows how the concentration gradients are affected by bulk precipitation. The higher precipitation rate constant, the slighter profiles. From equation 2.17 we get that a slighter profile results in a smaller mass transfer coefficient. This is represented in Figure 6.3. As we see here, the Sherwood number, which is the dimensionless mass transfer coefficient, decreases as the bulk precipitation rate constant increases. The high numbers near the inlet are due to the developing region. After the flow is stabilized, the coefficients straighten out.

6.4 Discussion

The simulations do not include a varying wall temperature and are therefore only applicable for flow loops. An implementation for varying wall temperature, such as encountered in subsea pipelines is needed for correct wax deposition modeling. Conductive heat transfer through the

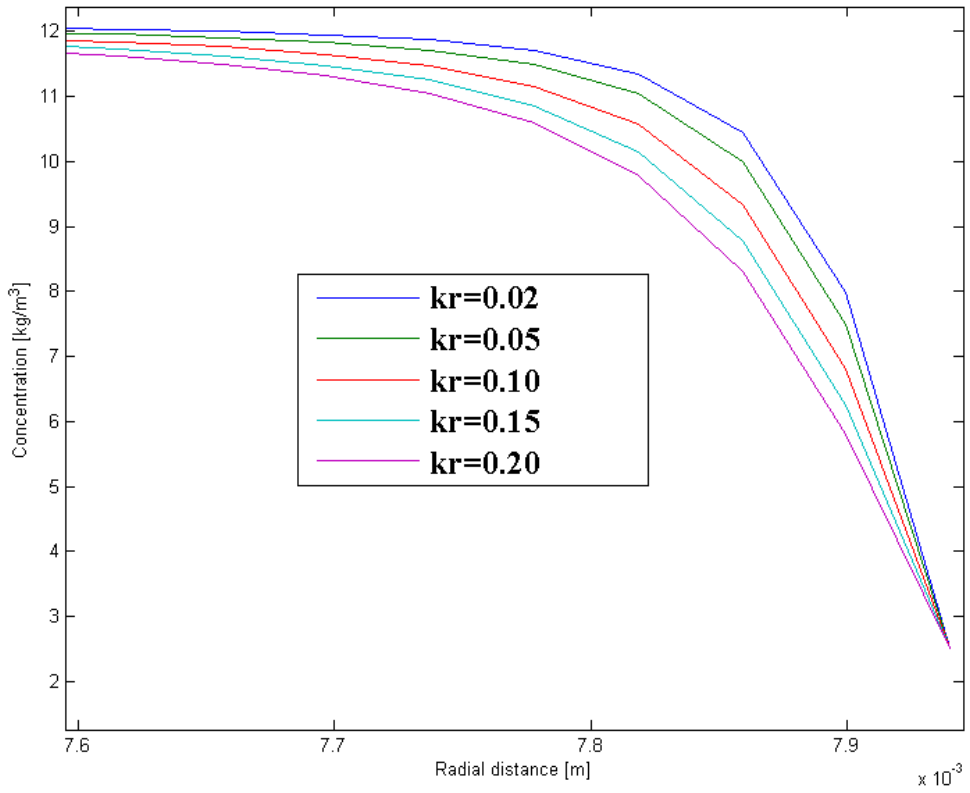

Figure 6.2: A plot of how the concentration profile near the wall changes as we increase the bulk precipitation rate constant.

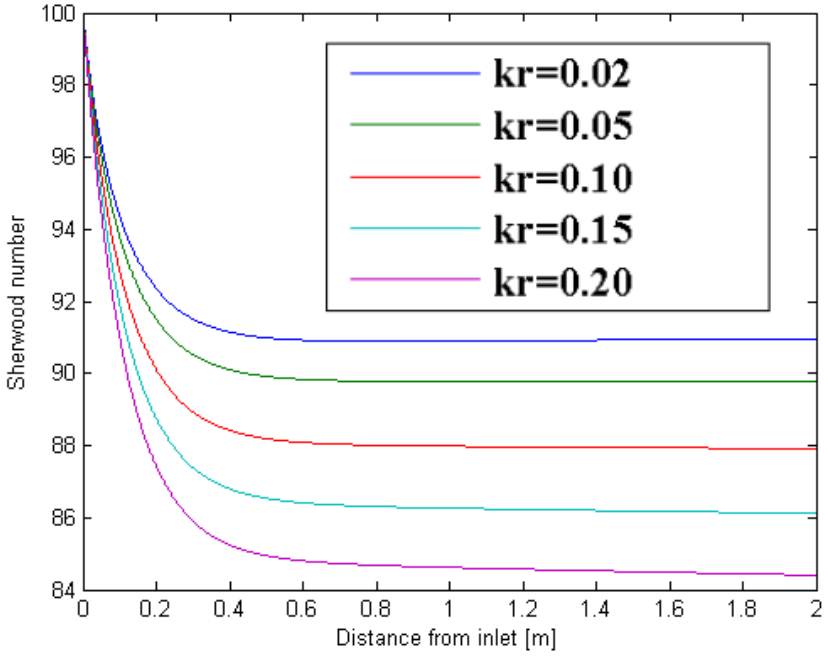

Figure 6.3: The Sherwood number versus distances from inlet as a function of the precipitation rate constant.

pipe wall and the deposit are needed to be calculated to obtain a correct inner wall temperature, see Figure 3.4.

Another particularity that is not implemented in the model, is a dynamic precipitation rate constant, k_r. As explained in Chapter 4.4 it varies with both viscosity and temperature. Since the temperature, hence also viscosity, varies both with radial and axial distance, a dynamic precipitation rate constant needs to be implemented.

7 Wax crystallites and crystallization

In order do achieve a better understanding of the precipitation kinetics of wax, we need to go down to the molecular level. For the behavior of suspended wax particles, the crystallites shape and morphology are relevant. This chapter gives an introduction to some of this theory.

7.1 Chemical characteristics of wax

In the petroleum industry, wax is a undesired high molecular alkane dissolved in the oil at reservoir conditions. They typically melts around 40-50$°C$. Waxes are ductile in nature, which means they somewhat deform under tensile stress instead of cracking. They are not amorphous, but has stable crystal structure at lower temperature. Its crystal structure is not rigid.

Alkanes are saturated hydrocarbons; it means that all the C-C bondings and C-H are *single* covalent bond. Its molecular form can be linear or branched, as seen in Figure 7.1, but linear shape is most common. In oil production context its carbon number ranges from 20 to 70. [1]. The amount of wax differs from crude to crude. Typically ranging from 1-15 wt% [38]. Wax crystal size varies with cooling rate, shear stress and composition[39]. Common particle size of bulk precipitated wax particles is 2-7μm[40]. A crystal of this size is known as a crystallite.

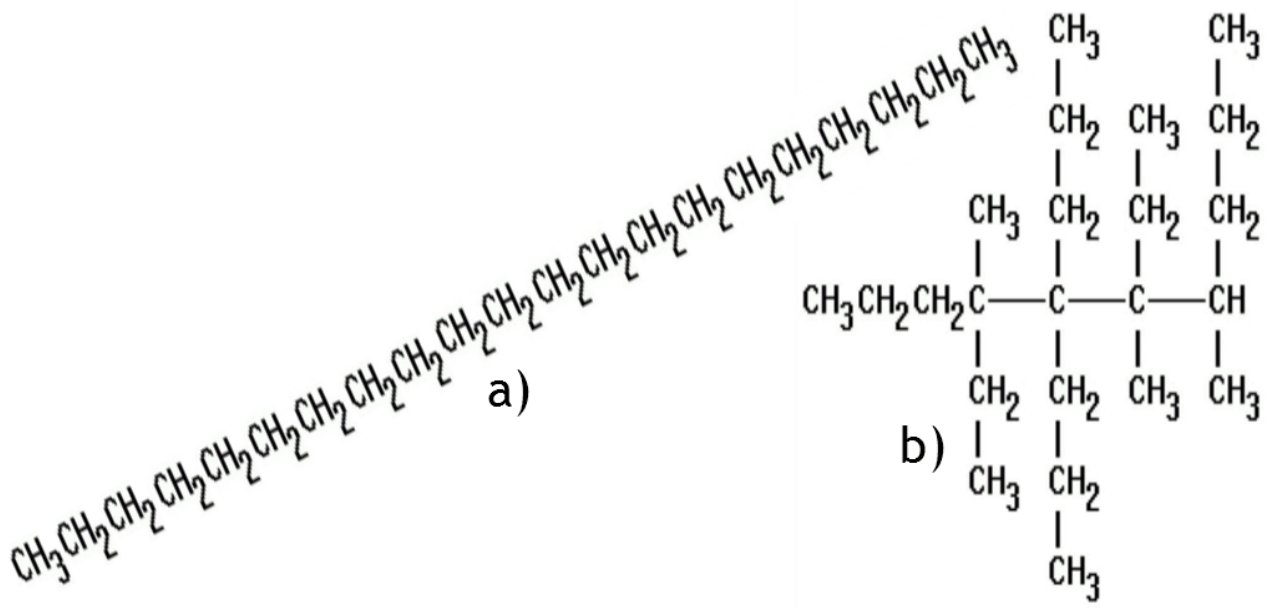

Figure 7.1: Paraffin wax molecules: a) linear, b) branched.

7.2 Intermolecular forces

Between molecules we have attractive and repulsive forces. The sum of these forces is known as van der Waals forces. As the temperature decreases, the movement of molecules is becoming more restricted by intermolecular forces. At sufficiently low temperature, the kinetic energy of the molecules are not big enough to move freely around anymore. The molecules cannot escape

each other and wax crystallizes. Branched alkanes have smaller surface area for intermolecular forces and their melting point is therefore less than non-branched alkanes.

For different molecules we have different intermolecular forces, some are stronger than other. Some of these forces depend on the anisotropic electrical charge, caused by octet rule. In wax molecules we have C-C bonds and C-H bonds, which both are single covalent. A slight polarity is caused by different electro negativity between hydrogen and carbon. Using Pauling's scale we find that the difference between hydrogen (2.2) and carbon (2.55) is 0.35. A number above 0.8 is required for a molecule to be polar. Hence, alkanes are non-polar.

7.3 Nucleus

In order to form crystals or crystallites there must exist a tiny solid body as basis for each crystal. In the crystallization theory the word nucleus is used. A nuclei can occur spontaneously in the solution known as homogeneous, or if induced by other particle present in the flow, heterogeneous[41]. A spontaneous nucleation requires a bigger supersaturation than growth on already existing nucleus. This is because spontaneous nucleation requires free energy in the solution to occur. In Figure 7.2 the solid line represent the solubility line. As the solution is cooled, it moves across the two lines into the metastable and labile zone and crystallization is allowed.

In an oil or condensate transporting pipeline there would always exist impurities such as tiny elements of the reservoir rock or corroded material from production equipment. Their existence are therefore making the crystallization process faster.

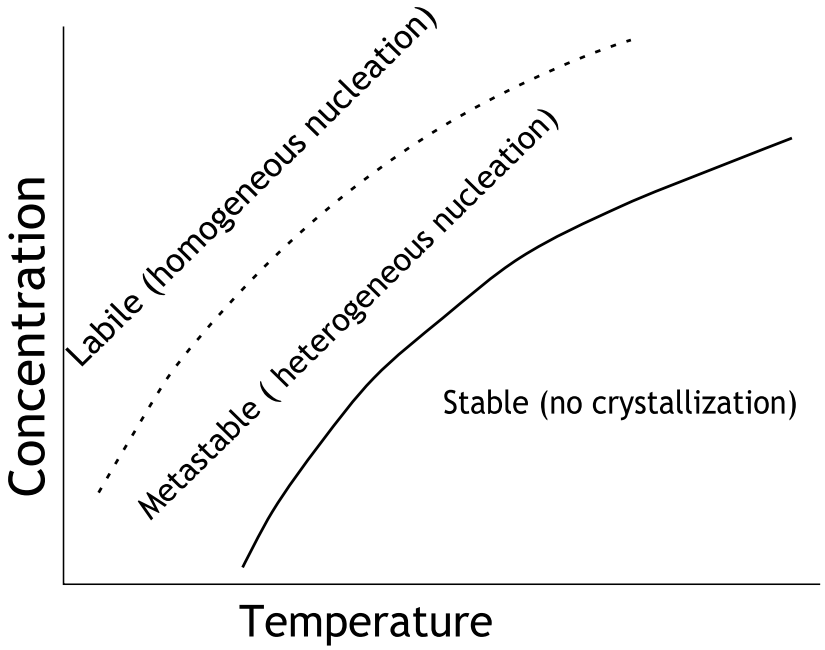

Figure 7.2: Stable, metastable and labile zone. The solid line represent the solubility and the dashed line represent nucleation line

For a nuclei to grow spontaneously we need free energy in the solution. A critical nucleus

size is the division above which nuclei can exist and below which nuclei will dissolve. This is determined by the amount of free energy in the solution. Lee(2008) determined the critical nuclei size to be $0.0123\mu m$ for the wax-oil mixture used[19].

7.4 Crystal growth

Growth of crystals are restricted by among other things, the mass transfer rate towards it. The mass transfer happens due to diffusion because of a decrease in saturation near the crystal's edge. The driving force is a supersaturation $C - C*$, see Figure 7.3 The supersaturation is "used" both for mass transfer towards the crystal, and for reaction with the crystal's edge[41]. Equation 2.24 describes the mass transfer towards a sphere. A wax crystallite is a long orthorhombic and the equation might need to be adjusted. In the simulations done in this thesis it is assumed that the particles move with the same speed as the fluid surrounding the crystallite. This means the mass transfer towards it is caused by diffusion alone. Turbulent mixing could increase this mass transport and the crystallization could happen faster. Crystallization rate of hydrates due to turbulent mixing is discussed by Mork[42, 34].

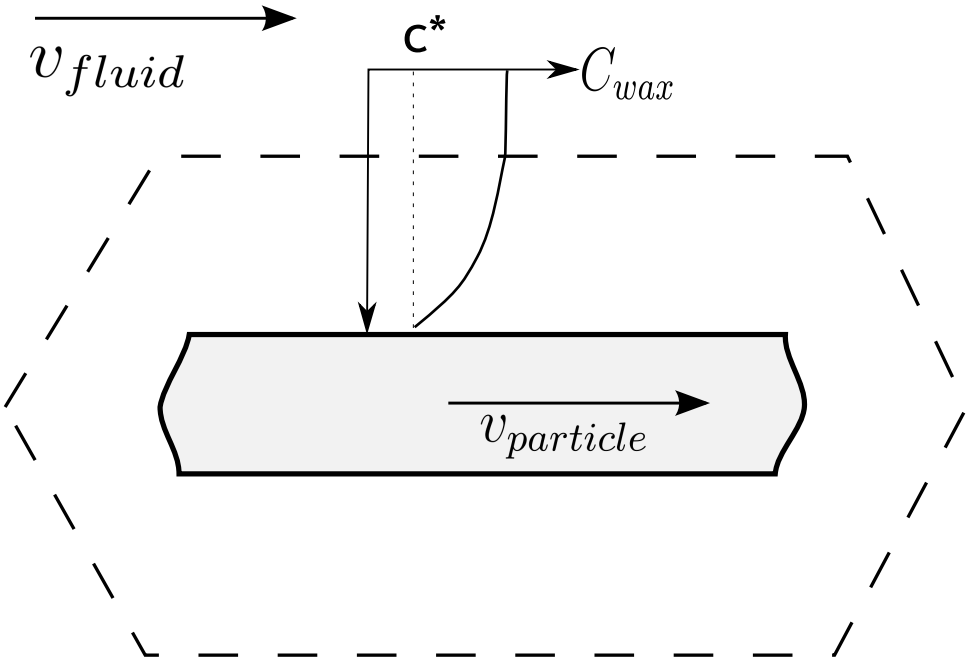

Figure 7.3: Supersaturation as the driving force for crystallite growth.

7.5 Wax crystallite morphology

A common way of deciding the shape of a crystal is by x-ray diffraction. When an x-ray beam hits an atom, its electrons make it scatter. By measuring the angel between the scattered x-rays one can decide the angles in the crystal structure. Understanding the shape of wax solid could give a better insight in wax particle-fluid behavior.

Such x-ray experiments done on paraffin waxes show that paraffin waxes (20 to 33 n-alkanes) with a continuous distribution of consecutive n-alkanes ($19 < n < 53$) forms a single orthorhombic solid solution[43]. When the alkanes are crystallized in binary or ternary molecular alloys, they can be triclinic and monoclinic. The latter is not relevant for our industry since we always get a multicomponent mixture from the reservoir. The important output for the scope of this thesis is that wax crystals are oblong and far from spherical.

The next question that arises is how oblong they are. This is measured in a aspect ratio. It is the width to length ratio of the wax crystallite, $\alpha = \frac{h_{wax\ particle}}{L_{wax\ particle}}$. See Figure 7.4 for illustration. The aspect ratio of wax crystallites in experiments performed by Venkatesan(2004) varies in the range 1-24[1]. When the flow rate goes up, the shear stress becomes stronger and the aspect ratio goes down[1]. With the presence of asphaltenes the aspect ratio of wax crystallites become smaller, which means that they become shorter and thicker[1]. It is important to mention that these observations are done in a wax deposit, and are not necessarily true for wax crystallites precipitated in the flow.

Experiments on how crystallite size varies with the cooling time has been preformed by Bakin et. al.[44]. The following relationship was found:

$$L_{max} \propto \left(\frac{dT}{dt}\right)^{-0.5} \tag{7.1}$$

Where L_{max} is the crystallite maximum length and $\frac{dT}{dt}$ is the cooling rate. Experiments done by Venkatesan in 2004 confirms this relation[1]. This equation applies to crystals formed in quiescent conditions. Particles formed in the bulk of the flow are formed under turbulent flow conditions, or if in the laminar sub layer, under high shear rates. So one can assume that the particles can be cracked in parts by eddies. The time for crystallization growth is also limited here. The particle might be tossed back into the core, where there exists no supersaturation for crystal growth.

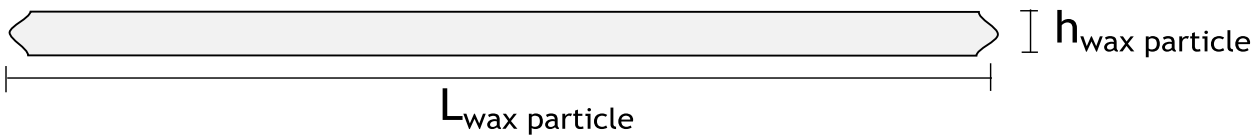

Figure 7.4: Aspect ratio of wax crystal. This particle has a aspect ratio of 24 and is the highest aspect ratio observed in Venkatesan's experiments[1].

8 Deposit porosity, growth and aging

The deposit does not only consist of wax. Studies of typical wax deposit in polarized light microscopes reveals that wax has platelet structures that overlap and interlock liquid oil, see Figure 8.1[16]. The amount of oil in the deposit is known as the wax porosity. It is calculated as the volumetric fraction of oil to the deposit total volume. Generally speaking, the higher porosity, the softer is the deposit. In laboratory experiments, the incipient wax layer might contain as much as 95% oil[1]. And Lund(1998) reports deposit wax fractions as high as 60-70% [45]. Since the deposit is a combination of both wax and oil, the term wax-oil gel is occationally used in experimental reports.

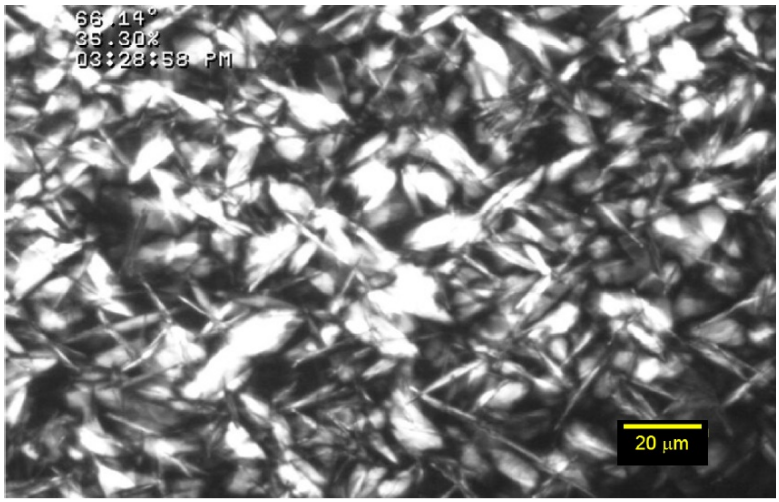

Figure 8.1: Polarized picture of wax crystals[19].

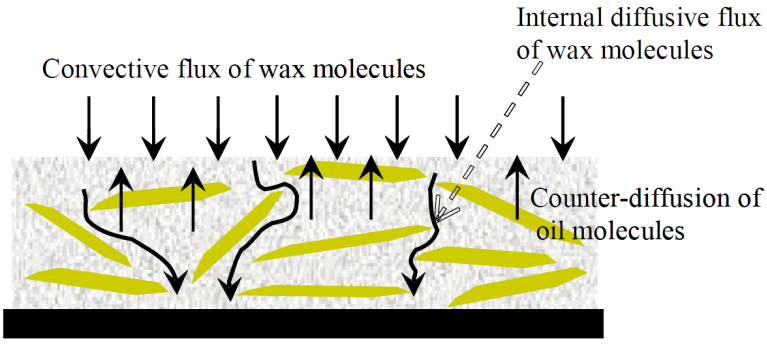

Figure 8.2: Illustration of how wax molecules diffuses into the deposit[1].

In early wax models, the wax porosity was considered time constant. According to Sing. et al(2000) the wax content of the deposit increases as time goes and wax diffuse into the deposit and oil is squeezed out[16]. In this case we distinguish between wax and oil with a critical carbon number. The paraffin molecules above this number diffuse into the deposit while those below diffuse out of the deposit. The concept is called aging. This makes the deposit harder as time goes on, thus the yield stress increases. The following equation is used to correlate deposit growth with the convective mass flux:[16]:

$$\overbrace{(-2\pi r_i)\rho_{gel}F_w\frac{dr_i}{dt}}^{\text{Rate of wax that contribute to thickness growth}} = \overbrace{(2\pi r_i)h_m(C_b - C_{wo}(T_i))}^{\text{Radial convective mass flux of wax molecules from bulk to the wax-oil interface}} - \overbrace{(2\pi r_i)\left(-D_e\frac{dC}{dr}\bigg|_i\right)}^{\text{Diffusive flux into the gel at the gel interface (responsible for aging)}} \tag{8.1}$$

ρ_{gel} is the deposit's density. $\frac{dC}{dr}\big|$ is the concentration gradient at the wall. The aging of a deposit is determined by the following equation[16]:

$$\pi\rho_{gel}(R^2 - r_i^2)\frac{dF_w}{dt} = -2\pi r_i\left(-D_e\frac{dC}{dr}\bigg|_i\right) \tag{8.2}$$

D_e is the effective diffusivity in the deposit, and are given by Aris (1985):[46, 19]

$$D_e = \frac{D_{wo}}{1 + R_2 + R_3 + R_4} \tag{8.3}$$

R_2, R_3 and R_4 are the resistances due to diffusion at their respective places as shown in Figure 8.3.

$$D_e = \frac{D_{wo}}{1 + \frac{\alpha^2 F_w^2}{1-F_w} + \frac{\alpha F_w}{\sigma} + \frac{4\alpha F_w}{\pi(1-F_w)}\ln\left[\frac{\pi\alpha^2 F_w}{\sigma(1-F_w)}\right]} \tag{8.4}$$

Where α is the crystals aspect ratio(width to thickness). F_w is given by:

$$F_w = \frac{(2d)^2 a}{(2d+s)^2(a+b)} \tag{8.5}$$

the lengths a, b, d, s are shown in Figure 8.3. The arrow shows a possible path for a wax molecule diffusing into the deposit.

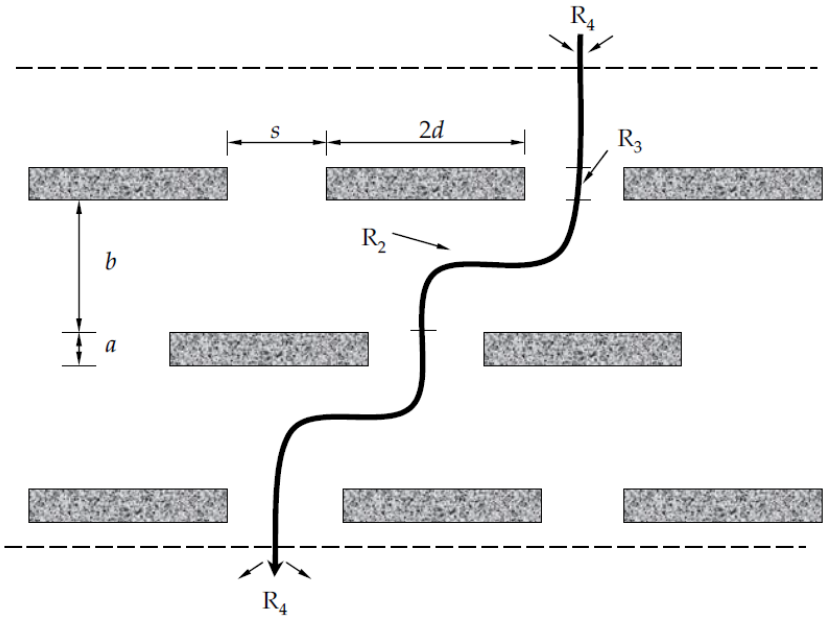

Figure 8.3: Deposits internal diffusion

9 Deposit hardness/strength

For pigging operations it would be valuable to obtain information about the deposits strength. Wax deposits strength is measured in yield stress, which is the maximum shear stress it can handle before it fractures. The strength is assumed to vary with the shear and thermal history of deposition[1].Hence, we can write the following relationship for the yield stress:

$$\tau_y = f(\tau_{gel}, \frac{dT}{dt}, \omega) \tag{9.1}$$

Where ω is the solid wax content of the deposit in weight-%, $\frac{dT}{dt}$ is the cooling rate and τ_{gel} is the shear stress the deposit was formed under. Venkatesan did important experiments on wax-oil gels, equivalent to wax deposits[1]. By studying the wax-oil gels in a microscope he found deposit strength to increase with both wax particle size and wax volumetric fraction. The wax particle size and wax amount are again dependent on the shear and cooling rates.

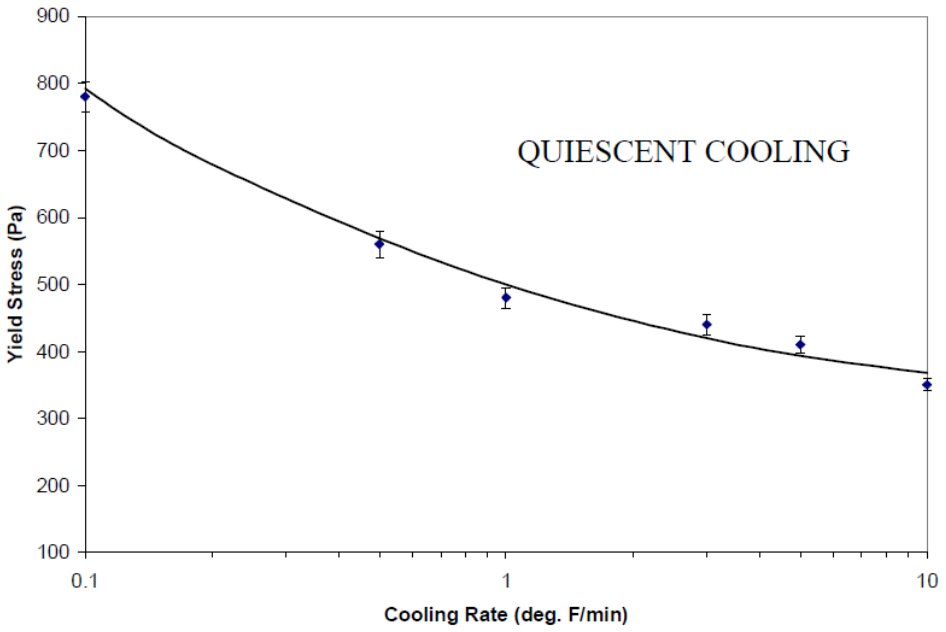

Figure 9.1: Yield stress under static conditions, different cooling rates[1].

Yield stress experiments were performed under different cooling rates, the result is shown in Figure 9.1 and Figure 9.2. As we see here, the shear stress yield decreases with increasing cooling rate under static conditions (no flow), but increases under dynamic conditions (flow).

Venkatesan explains these findings in the following way: Under static gelation conditions, a longer cooling rate provides longer time for crystal growth, resulting in bigger crystallites with bigger aspect ratio[1]. When applying a shear stress under the gel formation, the shear stress tends to break up the crystal as they form. In this way, the wax crystallites formed under lower cooling rates are exposed to the shear longer than under higher cooling rates. Hence, they becomes smaller, which in turn leads to weaker deposit.

Another important finding was done by plotting the yield stress under different shear stresses. Increased shear stress is equivalent with increased fluid velocity. As we see from

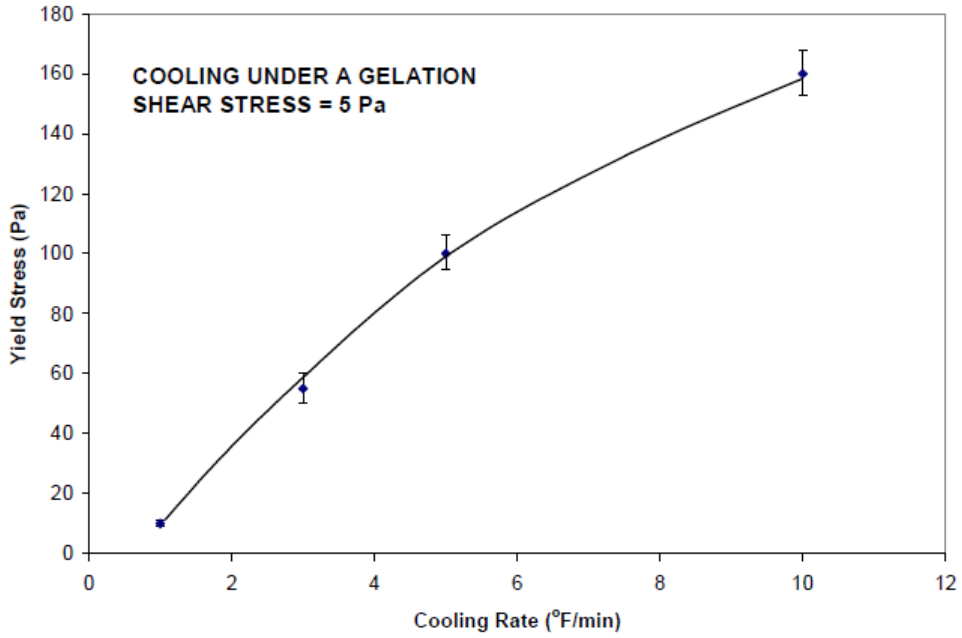

Figure 9.2: Yield stress under dynamic conditions, different cooling rates[1].

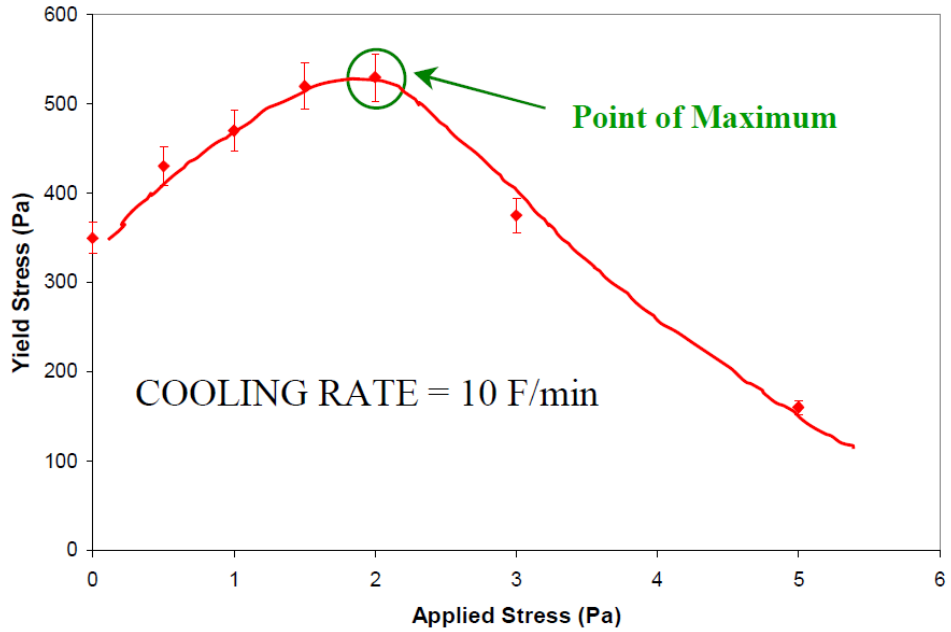

Figure 9.3: The deposit yield stress as a function of the yield stress applied under formation

Figure 9.3, the yield stress increases until a certain applied stress. After this certain applied stress, the yield stress is decreasing. This experiments were done for a variety of cooling rates, and are shown in Figure 9.4

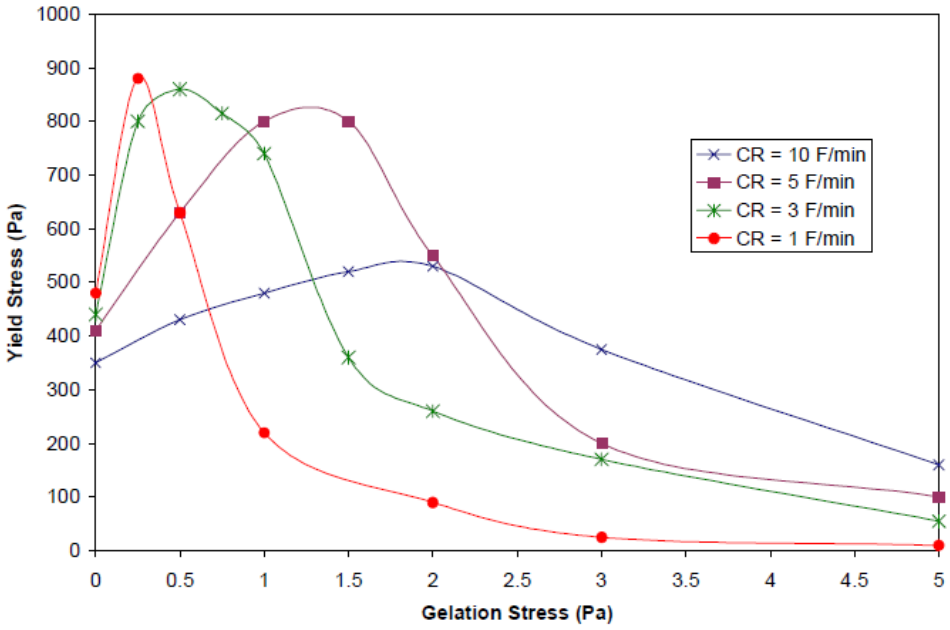

Figure 9.4: Yield stress under different cooling rates and shear stresses[1].

Venkatesan attempts to explain this in the following way: When a shear stress is applied to the deposit, the crystals tends to aggregate and form bigger crystals, which leads to stronger deposit, at a certain shear stress this trend turns: When applying further shear stress, the crystal is being broken down to smaller crystals with less aspect ratio. Since the yield stress is strongly dependent on the crystal size, the maximum yield stress could represent the applied stress where the crystal sizes reaches a maximum. Further increase in shear stress causes the crystals to be broken down to less crystals with lower aspect ratios which again leads to a deposit with less strength.

As the deposit ages, the wax content increase, this again leads to an increased strength. Deposits with different wax contents where tested for yield stress and the relationship is shown in Figure 9.5

These findings have important value for pigging engineering for crude oil pipelines. One would prefer the yield stress to be as low as possible. It is important to note that these findings is only valid for the oil-wax system used in these experiments, and the relationship cannot necessarily be extrapolated to other crude oil compositions. The yield stress can be related to the removal force required for pigging by[47]:

$$F_b = C_{bfc}\tau_y(\phi)\delta_d\pi D\eta(1-\phi) \tag{9.2}$$

Where F_b is the breaking force required, C_{bfc} is a breaking force coefficient, δ_d is the deposit thickness ϕ is the wax porosity and η is pig wax removal efficiency.

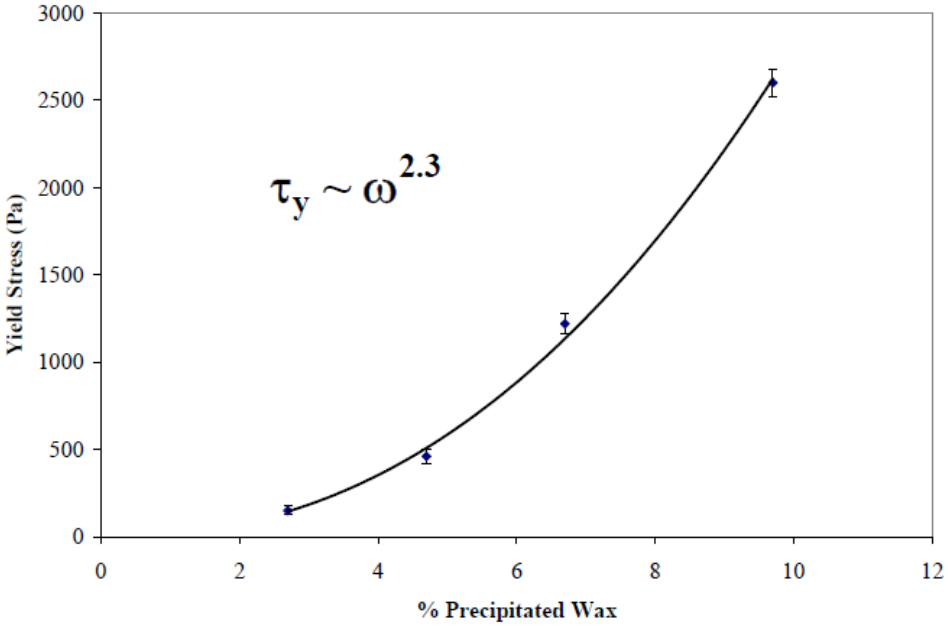

Figure 9.5: Yield stress as a function of the deposits wax content[1].

10 Shear dispersion

10.1 Historical background

In the context of wax deposition, the term shear dispersion was introduced by Bern et. al.(1980)[48]. Shear dispersion originates from the work done by Eckstein and Bailey on shear induced self-diffusion, which will be elaborated later on. Burger et. al.(1981) continued working with the concept and attempted to quantify it experimentally[40]. The deposition rate by shear dispersion was calculated by subtracting the total deposition from experiments with the theoretically calculated contribution from molecular diffusion.

The deposit growth contribution from shear dispersion was found to be larger than the contribution from molecular diffusion and was therefore concluded to be the main mechanism in wax deposition. After the publication, the work done by Burger has been criticized and the shear dispersion is now highly questioned. Many experiments have later on proved particle deposition not to be considered a contributing mechanism.

In this chapter two possible mechanisms causing dispersion of particles located in a shear flow are presented: Shear induced diffusion and shear induced lift.

10.2 Shear induced lift forces

When a fluid is flowing past the surface of a body, an unsymmetrical pressure distribution around the particle is formed. The flow field around the particle changes because of inertial effects, such as slip velocity and shear. In modern fluid dynamics the forces is summed up in two perpendicular forces, drag force and lift force. When a particle is exposed to a strong shear, the particle has different fluid velocity on each of its sides. Since the pressure is higher in the lower streamlines, the lift force is in the direction of increasing velocity.

A well-known shear induced lifting force is Saffmann Liftforce, which in 1964 was found to be equated as follows[49][2]:

$$F_{L(Saff)} = 1.615\mu V_s r_p^2 \dot{\gamma}^{1/2} \tag{10.1}$$

Where $\dot{\gamma}$ is the shear, also known as velocity gradient, $\frac{dV_f}{dr}$. V_s is the slip velocity and is defined as the difference in fluid velocity and particle velocity, $V_s = |V_p - V_f|$. r_p is the radius of the suspended particle radius.

The equation is only valid when the lift force contribution from shear is much greater than the contribution due to slip velocity. We must introduce a symbolic variable ε to represent the influence of one contribution to the other:

$$\varepsilon = \frac{Re_\gamma^{0.5}}{Re_s} \tag{10.2}$$

Where the two Reynolds numbers are:

[2]The equation constant was changed from 81 to 1.615 in 1968 after a mistake in his original paper was discovered.

$$Re_s = \frac{V_s d_p}{\nu} \tag{10.3a}$$

$$Re_\gamma = \frac{\dot{\gamma} d_p^2}{\nu} \tag{10.3b}$$

d_p is the particle diameter. For cases when the lifting effects caused by slip velocity become significant, the equation needs to be adjusted. This was studied by McLaughlin in 1991[50]:

When $0.025 < \varepsilon < 20$, the following relationship are valid:

$$\frac{F_L}{F_{L(Saff)}} = 0.3\Big\{1 + tanh[2.5\log_{10}(\varepsilon + 0.191)]\Big\}\Big\{0.667 + tan[6(\varepsilon - 0.32)]\Big\} \tag{10.4}$$

For even bigger ε, the deviation from Saffman is equated as follows[50]:

$$\frac{F_L}{F_{L(Saff)}} = -14.2\pi^2\varepsilon^5 \ln\left(\frac{1}{\varepsilon^2}\right) \tag{10.5}$$

It is important to emphasize that these equations apply to spherical particles only. Because wax particles are not spherical, but long orthorhombic, the lift force is assumed to deviate from the equations introduced for spherical bodies. The fluid dynamic calculations for a oblong orthorhombic becomes very complex and further study is required to draw any conclusions.

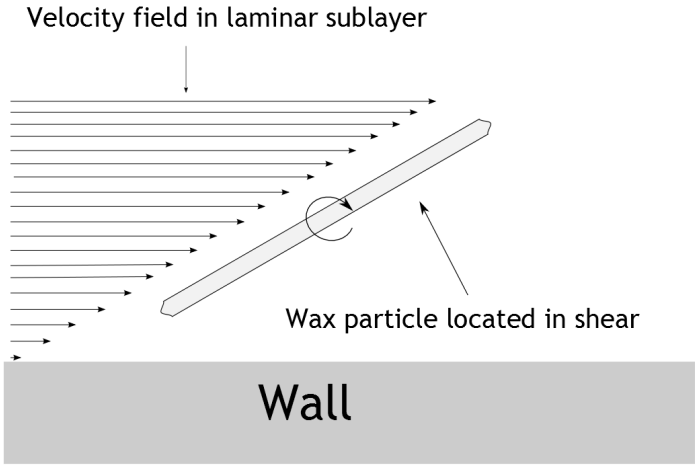

Figure 10.1: Long wax particle located in shear flow.

10.3 Shear induced self diffusion

Because of the presence of a velocity gradient, also known as the shear, particles might travel with different speed, determined by their distance from the wall. When a particle in a faster moving streamline is approaching another in an adjacent and slower moving streamline, they will eventually "collide". The quotation marks emphasize that a real collision between the

particles do not happen; it is the rotating fluid around the particles that "collide". Nevertheless, this interaction makes the two "colliding" particles to form a rotating duplet. The duplet rotates until the particle in a faster moving streamline is ahead of the one in the slower moving streamline, the duplet is then decomposed and they continue along with the flow in the streamline they originally were in. Therefore no radial migration. If a third particle interact with the duplet while rotating, a disturbance is made and the average radial displacement after the interaction is in the direction of decreasing concentration. The migration is therefore equivalent with diffusion, and can be described quantitatively by Fick's law.

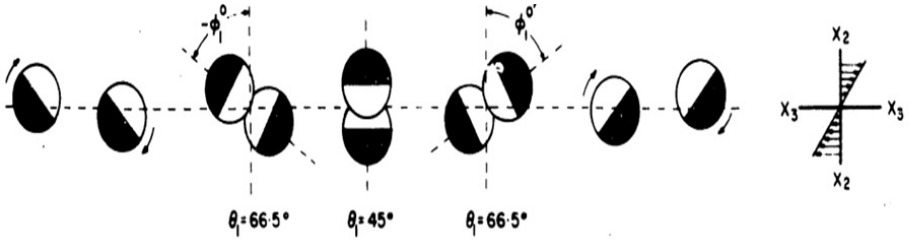

Figure 10.2: Two spherical particles colliding and rotating together[51].

The first attempts on quantifying the diffusion coefficient for self-diffusion was done by Eckstein(1975)[51]. He measured the radial migration of a radioactive particle in a particle suspension located in a shear. The following expression was found:

$$D_{si} = 0.020\alpha_p r_p^{1/2} \tag{10.6}$$

As we see, the mass flux caused by self-diffusion is dependent on the volumetric fraction of suspended particles. This differs from Brownian diffusion.

In the late 80's and beginning of 90's much work was done by Leighton and Acrivos, and Eckstein's equations were devolved further[52]. They included the fact that the shear rate near the wall is dependent of the particle concentration itself. An increase in particle concentration leads to an viscosity increase, hence an decrease in the shear. This in turn would decrease the migration due to shear induced self-diffusion. They introduced the following equation for the shear induced self-diffusion coefficient:

$$D_{si} = 0.33\alpha_p^2(1 + 0.5e^{8.8\alpha_p}) \tag{10.7}$$

Converting from diffusion flux is done by considering the particle mobility, which is defined as:

$$\lambda = v_p/F_p \tag{10.8}$$

Where v_p is the velocity attained by the particle by applying the forceF_p. Together with the drag coefficient from stokes law we obtain the following expression for the shear induced diffusion force:

$$F_{si} = -5.94\alpha_p^2(1 + 0.5e^{8.8\alpha_p})|\tau|\frac{d\alpha_p}{dr} \tag{10.9}$$

The absolute value around τ means that the direction of migration is independent of the direction of the velocity gradient, which the shear stress is defined from.

As explained earlier, shear diffusion require rotating particles. So, the same question as for the shear induced lift force, arises also here. To find out whether oblong orthorhombic wax particles rotates in a shear or not, further investigation is required. Computational fluid dynamic analysis (CFD) can be done.

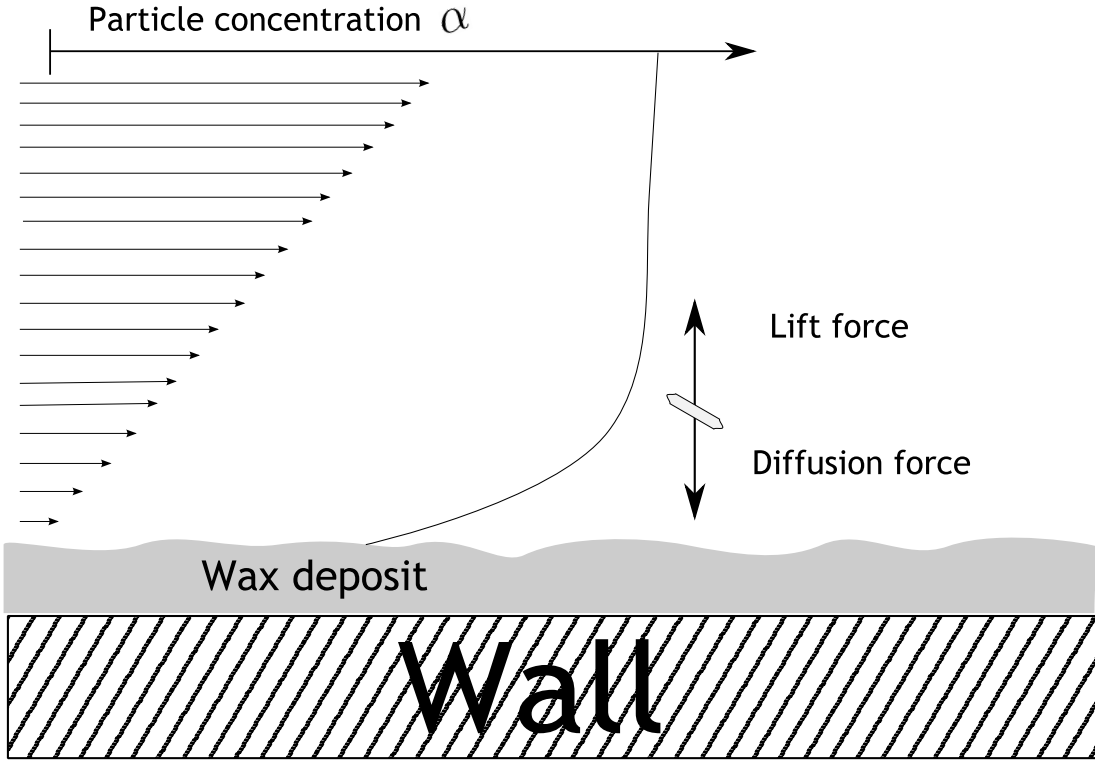

Figure 10.3: Forces acting on a particle in shear field with possible developed concentration gradient.

Since the temperature profile decreases towards the wall, wax particles precipitates here. The concentration gradient would therefore be increasing towards the pipe center. The obvious conclusion would therefore be that diffusion leads wax particles back into the turbulent core. But, after a while, the concentration in the core can be so big that diffusion must contribute to deposition towards the wall. Whether or not these particles stick to the wall or an already formed deposit, is another question to be answered.

10.4 Discussion

Two possible dispersion forces acting on particle located in a shear has been explained. A lift force favors dispersion away from the pipe wall and a diffusion force favors dispersion in direction of decreasing concentration. For a shear dispersion mechanism to be contributing to wax deposition, a sufficiently steep concentration gradient towards the wall must be present, see Figure 10.3. Particle distribution in fluid is a complex discipline. With oblong orthorhombic shaped crystallites instead of spherical, the analysis becomes even more difficult. How particles

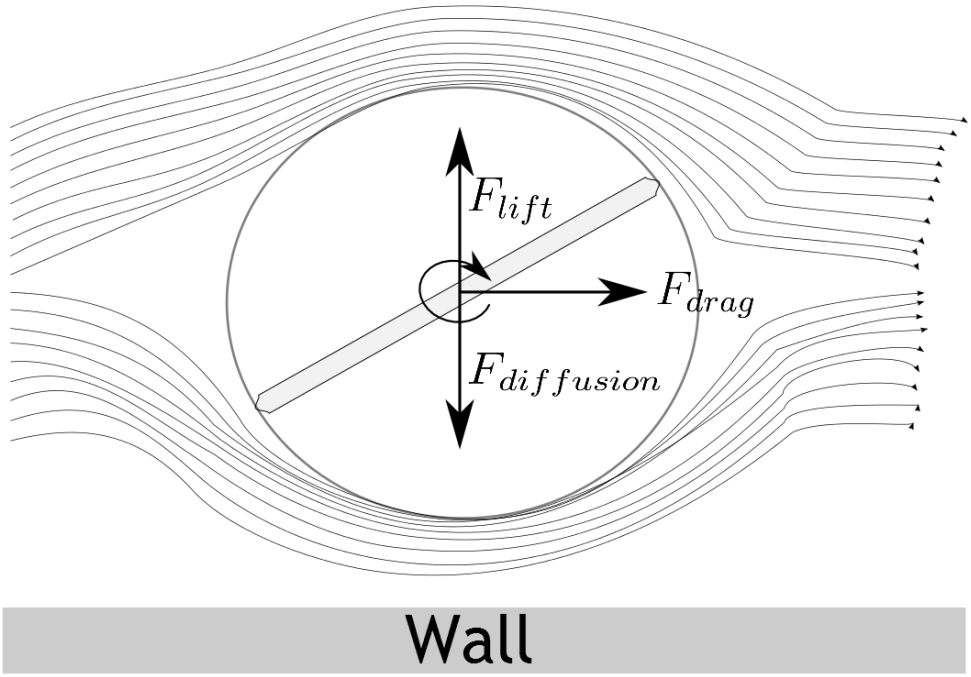

Figure 10.4: Possible streamlines around rotating particle.

are distributed in fluid flow are described in L. Zhao PHD thesis[53]. He discusses the near wall turbulent behavior of spheroid particles, which shape lies closer to oblong orthorhombic wax crystallites. This thesis might provide insights and equations for the shear dispersion phenomena.

11 Conclusions

An implementation of a method to calculate the mass transfer rate which is affected by bulk precipitation is done. The functions are shown in Appendix F. Simulations show that that bulk precipitation makes a slighter concentration gradient near the wall. This in turn makes the convective mass transfer coefficient less than what it would be without bulk precipitation. Experimental data shows that an increase in oil or condensate's flow rate leads to a slower paraffin build up[33, 1]. In the literature this is often explained by a removal effect, which arises when the shear grows larger. An increased precipitation rate due to the higher flow rate might be another explanation.

An elucidation of possible mechanisms causing shear dispersion is done. The equations presented by Burger et. al.[40], appear too shallow to apply for the oblong orthorhombic shape of wax crystallites. Investigations on their behavior and distributions in turbulent flow needs to be done to draw any conclusions[53].

12 Future work

In this thesis, the convective molecular mass flux from bulk to the wax-oil interface was simulated. Simulations together with the equations in Chapter 8 are needed to complete the wax deposition model. Lee(2008) describes the complete procedure for the model as follows:

" Computational model (Finite Difference Method combined with the wax prediction model by Singh et al., 2000[16])

1. Generate computational grids with given deposit thickness as a function of axial distance at a given time t.
2. Solve Equations 5.4 - 5.3 for laminar flow or turbulent flow to get axial temperature and concentration profiles.
3. Calculate the Sherwood number using Equation 2.17 and concentration profile obtained in (2).
4. Integrate Equations 8.1 and 8.1 to get new deposit thickness ($\delta_d(t+\Delta t)$) and wax fraction ($F_w(t+\Delta t)$).
5. Repeat (1)-(4) until time reaches the final time.

"

13 References

[1] R Venkatesan. *The Deposition and Rheology of Organic gels*. PhD thesis, University of Michigan, 2004.

[2] Sverre Ola Jonhsen Tore Prestvik and Haakon G. Rueslaatten. *Videregaaende geologi*. 1995.

[3] Offshore magazine. Deepwater challenges paraffins:. *http://www.offshore-mag.com/*. Cited: [26.06.2012].

[4] Hans Petter Rønningsen. Transportation of waxy crudes in multiphase pipelines. 03 2006. Cited: [20.06.2012].

[5] Pål Hedne. Subsea processing and transportation of hydrocarbons. page 19, 2012.

[6] M. D. C. Garcia and L. Carbognani. Asphaltene-paraffin strucutal interactions. effect on crude oil stability. *Energy and Fuels*, 15:1012–1027, 2001.

[7] Schlumberger Oilfield Glossary. Paraffin inhibitor. *http://www.glossary.oilfield.slb.com/Display.cfm?Term=paraffin%20inhibitor*. [Cited 02.07.2012].

[8] Statoil. Longer and colder, wax control for long step-out distances. 2012-01-19.

[9] L. Amundsen and R. Hoffmann. Method and device for measuring deposit thickness, 2011.

[10] M. Ilahi. Evaluation of cold flow consepts. Master's thesis, NTNU, 2005.

[11] V Tvedt. Evaluation of different commercialisation strategies for cold flow technology. Master's thesis, NTNU, 2006.

[12] F. Lund and M. Frøseth. *http://empig.no/*. Cited: [26.06.2012].

[13] L. F. A. Azevedo and A. M. Teixeira. A critical review of the Modeling of Wax Deposition Mechanisms. *Petroleum Science and Technology*, 21:393–408, 2003.

[14] K. Akbarzadeh and M. Zougari. Introduction to a novel approach for modeling wax deposition in fluid flows. 1. taylor-couette system. *Ind. Eng. Chem. Res.*, 47:953–963, 2008.

[15] Niesen V. G. Brown, T. S. and D. D. Erickson. Measurement and prediction of the kinetics of paraffin deposition. *SPE Annual Technical Conference and Exhibition, 3-6 October, Houston, Texas*, 1993.

[16] R. Venkatesan, P. Singh, and S. H. Fogler. Formation and aging of incipient thin film wax oil gels. *AIChE Journal*, 46(5):1059–1074, 2000.

[17] K. K. Botne. Modeling wax thickness in single-phase, turbulent flow. Master's thesis, NTNU, 2012.

[18] Senra M. Kapoor K. Huang, Z. and H.S. Fogler. Wax deposition modeling of oil/water. stratified channel flow. *AIChE Journal*, 57, No 4:841–851, 2010.

[19] Hyun Su Lee. *Computational and rheological study of wax deposition and gelation in subsea pipelines*. PhD thesis, The university of Michigan, 2008.

[20] M. Siljuberg. Shear dispersion: A misunderstood mechanism in solid deposition in pipelines? *NTNU*, 2011.

[21] M. Siljuberg. The bulk precipitation's impact on concentration driving force in wax deposition. *NTNU*, 2012.

[22] Warren E. Stewart R. Byron Bird and Edwin N. Lightfoot. *Transport Phenomena*. John Wiley & Sons,inc, 2002.

[23] Joel L. Plawsky. *Transport Phenomena Fundamentals*. Marcel Dekker, 2001.

[24] F.P. Incropera and D.P. Dewitt. *Fundamentals of Heat and Mass Transfer*, volume 5. 2002.

[25] E. L. Cussler. *Diffusion, Mass transfer in Fluid Systems*. Cambridge University Press, 2009.

[26] A. Cengel, Y and J.M. Cimbala. *Fluid Mechanics, fundamentals and applications*. Mc Graw Hill, 2010.

[27] P.H. Oosthuizen and D. Naylor. *Introduction to Convective Heat Transfer Analysis*. Mc Graw Hill, 1999.

[28] C. J. Geankoplis. *In Transport Processes and Separation Process Principles*. Prentice Hall, 2003.

[29] E. R. Van Driest. On turbulent flow near a wall. *AIAA Journal Special Supplement: Centennial of Powered Flight*, 23, 1956.

[30] M. S. Bhatti and R. K. Shah. *Handbook of Single-Phase Convective Heat Transfer*. Wiley-Interscience, 1987.

[31] Lee H. S. Fogler S. H. Huang, Z. and M. Senra. A fundamental model of wax deposition in subsea oil pipelines. *AIChE Journal*, 2011.

[32] J. S. Gudmundsson. Solids in oil and gas production. 1. draft, 2010.

[33] K. Rosvold. Wax deposition models. Master's thesis, NTNU, 2008.

[34] M. Mork. *Formation rate of natural gas hydrate*. PhD thesis, NTNU, 2002.

[35] R. Venkatesan and S. H. Fogler. Comments on analogies for correlated heat and mass transfer. *AIChE Journal*, 50 (7):1623–1626, 2004.

[36] A. K. Datta. *Biological and Bioenvironmental Heat and Mass Transfer*. CRC Press, 2002.

[37] Scientific blog. Please make a note. Cited: [26.06.2012].

[38] N. Aske. Wax - A flow assurance challange. 2007.

[39] Peters H. S. Torres R. A. Nagy N. A. Anderson, T. and D. L. Schruben. Wax crystal size distribution versus composition. *Fuel*, 80:1635–1638, 2000.

[40] Perkins T. K. Burger, E. D and J. H. Striegler. Studies of wax deposition in the trans alaska pipeline. *Journal of Petroleum Technology*, 33(6):1075–1086, 1981.

[41] J. W. Mullin. *Crystallization*. Butterworth Heinemann, 4 edition, 2001.

[42] M. Mork and J. S. Gudmundsson. Rate of hydrate formation in subesa pipelines. 2001.

[43] Chevallier V. Provost E. Mouroukba M. Dirand, M. and D. Petitjean. Multicomponent paraffin waxes and petroleum solid deposits: structual and thermodynamic state. *Fuel*, 77, 1998.

[44] Romanenko V. N. Schilz J. Nikitina G. V. Bakin, A. S.. and D. I. Ivanov. Sizes of crystallites as a function of the cooling rate. *Scr Metall Mater*, 31:1131–1134, 1994.

[45] Hans-Jacob Lund. Investigation of paraffin deposition during single-phase liquid flow. Master's thesis, The University of Tulsa, 1998.

[46] R Aris. On the permeability of membranes with parallel but interconnected pathways. *Math. Biosci*, 44:2781, 1985.

[47] SPT-Group. Olga user manual, version 7. page 105, 2011.

[48] Withers V. R. Bern, P. A. and R.J.R Cairns. Wax deposition in crude oil pipelines. *Proc. Eur. Offshore Pet. Conf. Exhib., London*, 571, 1980.

[49] P. G. Saffman. The lift on a small sphere in a slow shear flow. *Journal of Fluid Mechanics*, 22 (2):385–400, 1965.

[50] J. B. McLaughlin. Inertial migration of a small sphere in linear shear flows. *Journal of Fluid Mechanics*, 224:261–274, 1991.

[51] E. C. Eckstein. *Particle migration in a linear shear flow, PHD thesis*. PhD thesis, Massachusetts Institute of Technology, 1975.

[52] D. Leighton and A Acrivos. Measurement of shear induced self diffusion in concentrated suspension of spheres. *Journal of Fluid Mechanics*, 177:109–131, 1987.

[53] Lihao Zhao. *Particles in wall turbulence*. PhD thesis, NTNU, 2011.

[54] A. D. McNaught and A. Wilkinson. *Compendium of Chemical Terminology*. International Union of Pure and Applied Chemistry, 1997.

[55] C. R. Wilke and P. Chang. Correlation of diffusion coefficients in dilute solutions. *AIChE Journal*, 1 (2), 1955.

[56] W. Hayduk and B. S. Minhas. Correlations for prediction of molecular diffusivities in liquids. *The Canadian Journal of Chemical Engineering*, 60(2):295–299, 1982.

[57] J. S. Gudmundsson. Cold flow hydrate technology. *4th International Conference on Gas Hydrates, May 19-23, 2002, Yokohama*, 2002.

[58] Prashant T., Steven P. A, and Michael Z. P. Modeling shear-induced diffusion force in particulate flows. *Computers & Fluids*, 38:727–737, 2009.

Appendices

A Derivation of the solubility method

A method to determine the Sherwood number by including the solubility of wax in oil was done by Venkatesan[1]. As discussed in Chapter 2.3, the convective heat and mass transfer coefficients are empirical variables that allow us to compute the heat and mass transfer as a function the temperature and concentration difference between the wall and bulk. From Fourier's and Fick's law we get that the heat and mass transfer through the pipe wall is equal to the temperature or concentration gradient at the wall multiplied with the thermal diffusivity or diffusion coefficient. Combining these equations, we get:

For heat transfer:

$$h\Delta T = -k\left(\frac{dT}{dr}\right)_{wall} \tag{A.1}$$

For mass transfer:

$$h_m\Delta C = -D_{WO}\left(\frac{dC}{dr}\right)_{wall} \tag{A.2}$$

By using the definitions of Nusselt and Sherwood number we get the following equations:

$$Nu = \frac{2r}{\Delta T}\left(-\frac{dT}{dr}\right)_{wall} \tag{A.3}$$

$$Sh = \frac{2r}{\Delta C}\left(-\frac{dC}{dr}\right)_{wall} \tag{A.4}$$

We divide the two equations on each other:

$$\frac{Sh}{Nu} = \frac{\left(\frac{dC}{dr}\right)_{wall}}{\left(\frac{dT}{dr}\right)_{wall}}\frac{\Delta T}{\Delta C} \tag{A.5}$$

The concentration at the solid-fluid interface can be calculated as a function of temperature: $C_{wo} = f(T)$. By using the chain rule on Equation A.5 we obtain the following equation for the dimensionless convective mass transfer coefficient:

$$Sh = Nu\frac{dC_{wo}}{dT}\frac{T_{bulk} - T_{wall}}{C_{w,bulk}(T) - C_{w,wall}(T)} \tag{A.6}$$

B Temperature dependency of viscosity

In Chapter 4.4 we try to derive a quantitative measure of bulk precipitation of wax particles. In order to do it correctly, a temperature dependent equation for the diffusion coefficient, hence also viscosity is needed. This appendix shows the correlations used for the equations in Chapter 4.4.

From everyday experience we know that the viscosity of a substance decreases with increasing temperature. Viscosity is a measure of a fluids resistance to flow. It is a result of the cohesive forces (forces of attraction) between the molecules in the fluid. As the temperature increases, molecules moves faster and the amount of time molecules stays "in contact" with each other becomes less. Thus, these cohesive forces become smaller compared to the molecular momentum transfer between molecules and the viscosity is reduced.

Svante Arrhenius developed an equation to describe temperature dependence of a chemical reaction constant. Both viscosity and the speed of a chemical reaction is determined by the interactions between molecules (or reactants), therefore this equation has also shown to be valid for the temperature dependency of viscosity. The equation he introduced is [54]:

$$k = A_r \exp\left(\frac{-E}{RT}\right) \tag{B.1}$$

A is the pre-exponential factor and the latter is basically the Boltzmann factor, where E is activation energy and R is the universal gas constant. For viscosity:

$$\mu = A_\mu \exp\left(\frac{E}{RT}\right) \tag{B.2}$$

Where A_μ is a viscosity coefficient for the respective material. The inversion of the Boltzman factor is due to the fact that less molecular interactions give higher viscosity. Since we are only interested in the viscosity dependency from a reference viscosity we can divide two copies of Equation B.2 at different temperatures on each other and we obtain:

$$\mu = \mu_{cloud} \exp\left[\frac{E}{R}\left(\frac{1}{T} - \frac{1}{T_{cloud}}\right)\right] \tag{B.3}$$

C Diffusion coefficient and its temperature and viscocity dependency

The diffusive mass flux is dependent of the solvents temperature and viscosity. This is reflected through the diffusion coefficient which correlation is described in this appendix. A high viscosity means that the cohesive forces between molecules are significant, which makes it more difficult for molecules to move. That is due to more molecular activity and the diffusion may happen faster.

There has been developed a many empirical correlations trying to describe the dependency, and the equation for chemical reaction constant which was used for the viscosity can also be used for the diffusion coefficient. In the SPE-literature especially two equation stand out: Wilke & chang(1955)[55]:

$$D_{wo} = 7.4 \cdot 10^{-12} \frac{(xM)^{1/2} T}{\mu V_{bp}^{0.6}} \tag{C.1}$$

Hayduk Minhas (1982)[56]:

$$D_{wo} = 13.3 \cdot 10^{-12} \frac{T^{1.47} \mu^{\gamma}}{V}, \gamma = \frac{10.2}{V} - 0.791 \tag{C.2}$$

x is an association parameter, multiple of nominal molecular weight of solvent to give effective value. M is the molecular weight, μ is the viscosity of solution, V is the molar volume of solute and V_{bp} is the molar volume at normal boiling point. In this project the Hayduk Minhas correlation was used. Typical values of the binary diffusion coefficient in hydrocarbons mixtures are in the range $0.1 \cdot 10^{-9} < D_{wo} < 10 \cdot 10^{-9}$[32].

D Particle suspension influence on viscosity

The suspension of particles in a fluid is increasing its effective viscosity. This could cause additionally pressure loss and therefore higher power requirement for pumping. When the amount of suspended particles in the flow exceeds a certain limit, the fluid is no longer able to flow. This is called pour point temperature. Figure D.1 shows different models for the the apparent viscosity increase as a function of the volume fraction. It is reasonable to believe that an increase in volume fraction of oblong particles affect viscosity more than for spherical particles; oblong particles have a larger surface-volume ratio.

Studies on hydrate slurries was done by Gudmundsson[57]. He concluded that particle suspension viscosity increase do not influence the pressure loss in the turbulent flow regime. This is because the particles is kept in the turbulent core due to lift forces in the sub layer. The pressure loss in a turbulent flowing pipe is caused with the flows contact with the wall. If it is no viscosity increase in the fluid in contact with the wall, the overall pressure loss will not increase.

$$\mu_a = \mu_0 \hat{\mu} \tag{D.1}$$

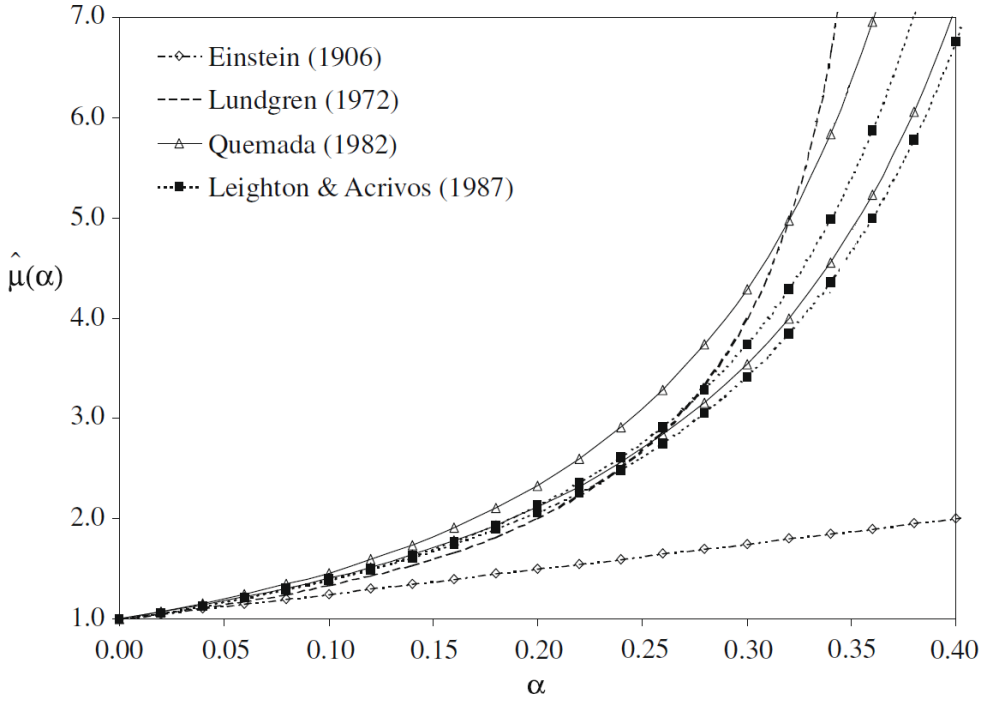

Figure D.1: Viscosity as a function of volume fraction of particles[58].

E Wax deposition modelling in AspenTech HYSYS

AspenTech HYSYS is a process modeling tool for conceptual design or optimization of different processes. Its pipe module contains wax deposition models. Hysys's standard chemical element package does not support n-alkanes higher than C_{30}. In many waxy crudes we have alkanes up to as much as C_{70}. To add additionally components in HYSYS we include something HYSYS calls hypothetical components. We have to feed HYSYS with their thermodynamic properties. As a minimum HYSYS accept an input of natural boiling point, molecular weight and the liquid density. Then HYSYS will estimate the necessary properties that HYSYS needs to run simulations of a fluid. The hypothetical components are added in "Hypo Manager" located in the component list, see Figure E.1.

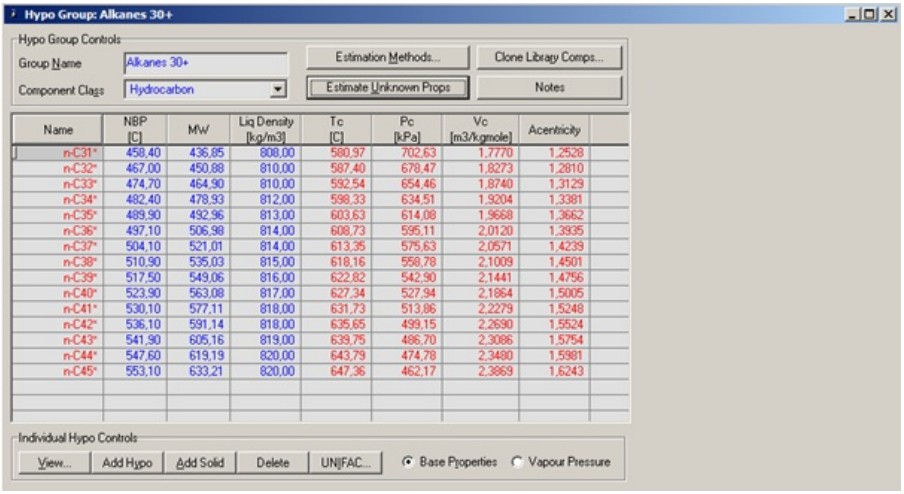

Figure E.1: Including hypothetical components to HYSYS.

Properties was obtained from http://www.chemspider.com/ and are shown in the Table E. When the hypothetical components are added, you enter the simulation environment and create a flow through a pipe and enters the heat transfer specifications.

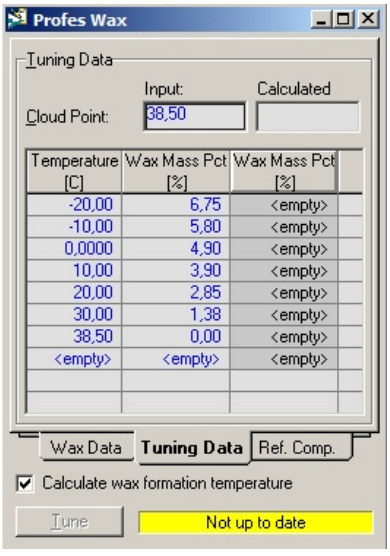

Figure E.2: Defining the precipitation curve. These values are from Norne crude.

Alkane	Natural boling point (k)	Molecular weigth	Liquid density $\left(\frac{kg}{m^3}\right)$
n-C31	458,4	436,9	808
n-C32	467,0	450,9	810
n-C33	474,7	464,9	810
n-C34	482,4	478,9	812
n-C35	489,9	493,0	813
n-C36	497,1	507,0	814
n-C37	504,1	521,0	814
n-C38	510,9	535,0	815
n-C39	517,5	549,1	816
n-C40	523,9	563,1	817
n-C41	530,1	577,1	818
n-C42	536,1	591,1	818
n-C43	541,9	605,2	819
n-C44	547,6	619,2	820
n-C45	553,1	633,2	820

Table 2: Properties of higher alkanes.

In the pipe segment window, go to the "Deposition" tab, here you can specify the time interval and the total deposition time to be calculated for. Select "Profes" and click "View Method". Under the "Wax data tab", you choose the preferred wax deposition model. Do also make sure that all the wax components are marked. Under the "Tuning tab" you enter the oils precipitation curve, temperature versus precipitated solid wax fraction, see Figure E.2. Now you go to the "profile" tab under Deposition and enter the initial deposit thickness, typically 0 for all the segments.

You will now find your deposition profile under Performance-profiles-"view profile". The numerical values are found under Profile in the Deposition tab. See Figure E.3 for a typical profile made by HYSYS.

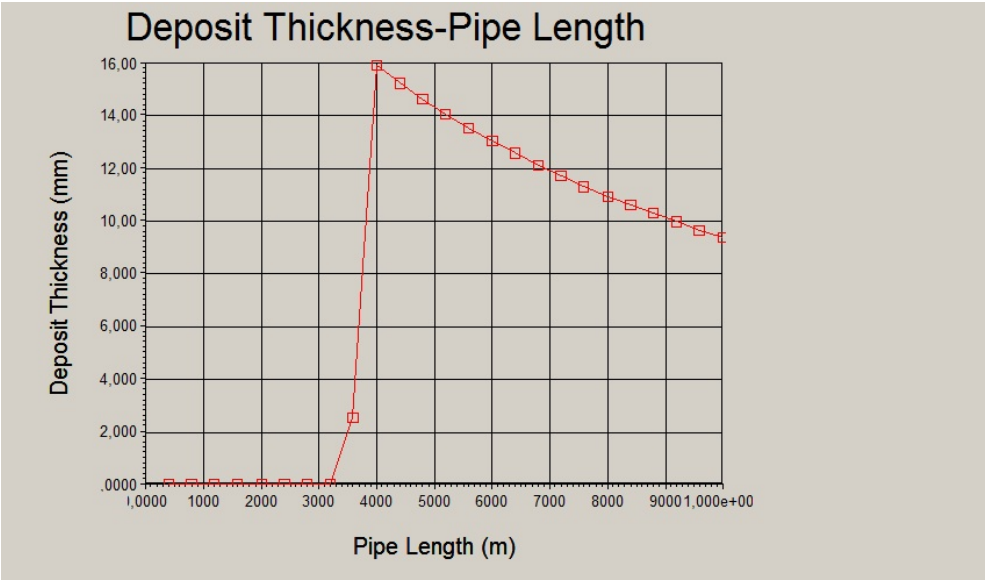

Figure E.3: Deposition profile output from HYSYS.

F Matlab script for numerical calculations of Sherwood number

Matlab Script 1 Matlab function for creating the concentration matrix. We need to produce a new coefficient matrix for each axial step.

```
function [ C ] = ...
    concentration_calc(ni,nj,R,L,Q,nu,Tw,Ti,T,kr,turbulent,mu,Va)
% T is the temperature matrix
% Initializing the grid
dr=R./nj;           % Differential in radial direction
dz=L/ni;            % Differential in lateral direction
C = zeros(nj,nj);   % Concentration grid
Cw=solubility(Tw);  % Concentration at the wall
Ci=solubility(Ti);  % Concentration at the inlet
C(:,1) = Ci;        % Setting inlet concentration in the grid

%***********Iterating over the pipe from inlet to outlet******************

D_C=ones(nj,1); D_C(1)=0; D_C(nj)=Cw; % Making D-vector
A_C=zeros(nj,nj-1); A_C(1,1)=1; A_C(1,2)=-1; A_C(nj,nj)=1;%Coefficient matrix
for i=2:ni
    for j=2:nj-1
        % Making mass diffusivities at different radial positions:
        Dwo1=Dwo_tot(dr,(j-1),i); %Dwo_i-1
        Dwo2=Dwo_tot(dr, (j) ,i); %Dwo_i
        Dwo3=Dwo_tot(dr,(j+1),i); %Dwo_i+1
        vz=Velocity(j*dr,R,Q,nu,turbulent);
        %Making a new coefficient matrix for each axial step
        A_C(j,j-1)=-1/(2*j*dr^3)*(j*dr*Dwo2+(j-1)*dr*Dwo1);%C_T
        A_C(j,j)=vz/dz+1/(2*j*dr^3)*(2*j*dr*Dwo2+(j+1)*dr*Dwo3+(j-1)*dr*Dwo1)+kr;%A_T
        A_C(j,j+1)=-1/(2*j*dr^3)*((j+1)*dr*Dwo3+j*dr*Dwo2);%B_T
    end
    for j=2:nj-1 % Making D_C-vector
        vz=Velocity(j*dr,R,Q,nu,turbulent); % Velocity as a function of r
        D_C(j)=C(j,i-1)*vz/dz+kr*solubility(T(j,i));  % D_C
    end
   C(:,i)=A_C\D_C; % Matlab solves the linear system
   C(1,i)=C(2,i);
end

function [ Dwo_tot ] = Dwo_tot(dr,j,i)
%Calculates the total mass diffusivity at a given radial and axial distance

% Calculating the diffusion coefficient from Hayduk Minhas correlation
gamma=10.2/Va-0.791;
Dwo=13.3*10^-12*T(j,i)^1.47*mu^gamma/Va^0.71;

Sc=nu/Dwo;
Sc_T=0.85+0.015/Sc;
Dwo_tot=Dwo+eddyDiffusivity(j*dr,R,Q,nu,dr)*Sc/Sc_T*Dwo;
end

end
```

Matlab Script 2 Matlab function for creating the temperature matrix.

```
function [T] = temperature_calc(ni,nj,R,L,Q,nu,Tw,Ti,alpha0,turbulent )
% Initializing the grid
dr=R./nj;            % Differential in radial direction
dz=L/ni;             % Differential in lateral direction
T = zeros(nj,nj);    % Temperature grid
T(:,1) = Ti;         % Setting inlet temperature in the grid

%% ************************TEMPERATURE PROFILE*****************************
Pr=nu/alpha0;        % Prandlt number

%**************Producing the coefficient matrix*****************************
%Initializing the coefficient matrix:
A_T=zeros(nj,nj-1); A_T(1,1)=1; A_T(1,2)=-1; A_T(nj,nj)=1;

for j=2:nj-1
    % Making thermal diffusivities at different radial positions:
    alpha1=alpha_tot(dr*(j-1)); %alpha_i-1
    alpha2=alpha_tot(dr* (j) ); %alpha_i
    alpha3=alpha_tot(dr*(j+1)); %alpha_i+1
    vz=Velocity(j*dr,R,Q,nu,turbulent);

    %Writing the coefficient matrix:
    A_T(j,j-1)=-1/(2*j*dr^3)*(j*dr*alpha2+(j-1)*dr*alpha1);%C_T
    A_T(j,j)=vz/dz+1/(2*j*dr^3)*(2*j*dr*alpha2+(j+1)*dr*alpha3+(j-1)*dr*alpha1);%A_T
    A_T(j,j+1)=-1/(2*j*dr^3)*((j+1)*dr*alpha3+j*dr*alpha2);%B_T
end
%************Iterating over the pipe from inlet to outlet*****************
D_T=ones(nj,1); D_T(1)=0; D_T(nj)=Tw; % Making D-vector
for i=2:ni % z-direction
    T(nj,i)=T(nj,i-1);
    T(nj-1,i)=T(nj,i-1);
    for j=2:nj-1 %Making D-matrix
        vz=Velocity(j*dr,R,Q,nu,turbulent);
        D_T(j)=T(j,i-1)*vz/dz;  %D_T
    end
   T(:,i)=A_T\D_T; % Matlab solves the linear system
   T(1,i)=T(2,i);
end
function [ alpha_tot ] = alpha_tot(r)
%Calculates the total thermal diffusivity
Pr_T=0.85+0.015/Pr;
alpha_tot=alpha0+eddyDiffusivity(r,R,Q,nu,dr)*Pr/Pr_T*alpha0;
end
end
```

Matlab Script 3 Function for the solubility.

```
function [ solubility] = solubility( temperature )
% Calculates the the solubility of wax in oil at a certain temperature
% This solubility curve is a digitilized version of Norne crude and it
% should be replaced by a solubility curve for the oil investigated.
solubility= 0.0007*temperature^2 + 0.0989*temperature + 1.7706;
end
```

Matlab Script 4 Function for calculating the eddy diffusivity.

```
function [ eddyDiffusivity ] = eddyDiffusivity(r,R,Q,nu,dr)
% Calculates the eddy diffusivity at a given radial position.
% y_p  - Represents the dimensionless distance from the wall, y+
% vz_p - Dimensionless turbulent velocity
Re=2*Q/(pi()*R*nu);
f=0.305/Re^0.25;
k=0.4;
A=26;
y2=y_p(r+dr);          % Dimensionless distance at r+dr
y1=y_p(r);             % Dimensionless distance at r
dv=vz_p(y2)-vz_p(y1);% Dimensionless velocity difference between y2 and y1
dy=y2-y1;              % Difference
dvdy=dv/dy;            % Derivative of dimensionless velocity to ...
    dimensionless distance

% Van Driest's equation for the eddy diffusivity:
eddyDiffusivity=(k.*y_p(r)).^2.*(1-exp(-y_p(r)/A)).^2.*dvdy;

function vz_p = vz_p( y_p )
    % Calculates the dimensionless turbulent velocity as a function of the
    % dimensionless wall distance
    if (y_p<=5)
        vz_p=y_p;
    elseif (5<=y_p<=30)
        vz_p=5*log(y_p)-3.05;
    else
        vz_p=2.5*log(y_p)+5.5;
    end
end

function y_p=y_p(r)
    % Calcualtes the dimensionless distance from the wall as a function of
    % radius
    y_p =(1-r/R)*Re/2*sqrt(f/8);
    end
end
```

Matlab Script 5 Function for calculating the velocity profile.

```
function [ Velocity ] = Velocity( r,R,Q, nu, turbulent)
%Calculates the velocity for a given radial position r.
% r  - Radial distance of interest                [m]
% R  - Pipe's total radius                        [m]
% Q  - Flow rate                                  [m^3/s]
% nu - Oil or condensate's kinematic viscosity    [m^2/s]
% Turbulent - Logical operator, true forces turbulence
% Vm - Pipe's average velocity
% Re - Reynolds number

vm=Q/pi()/R^2;
Re=2*Q/pi()/R/nu;
%*************************** Laminar flow******************
if(Re>4000&&turbulent==false)
    Velocity = 2*vm*(1-(r/R)^2);
    return;
end
%**********************Turbulent flow***********************
y=R-r;
f=0.305/Re^0.25;
y_p =(1-r/R)*Re/2*sqrt(f/8);
if (y_p<=5)
    vz_p=y_p;
elseif (5<=y_p<=30)
    vz_p=5*log(y_p)-3.05;
else
    vz_p=2.5*log(y_p)+5.5;
end

Velocity=vz_p*nu/y*(1-r/R)*Re/2*sqrt(f/8);
end
```

Matlab Script 6 Script for plotting the figures.

```
%%  **********************Definning the grid*******************************
ni = 30;              % Grid size in lateral direction
nj = 200;              % Grid size in radial direction
R=0.00794;              % Pipe radius
L=2;                   % Pipe length
%********************Temperature inputs************************************
Tw = 7;                % Wall temperature
Ti = 70;               % Inlet temperature
%********************Fluid properties inputs*******************************
alpha0=9.8*10^-7;      % Thermal diffusivity of wax-oil mixture
Dwo_0=4*10^-9;         % Mass diffusivity of wax in oil
Q=0.00063;                % Flow rate [m^3/s]
nu=4.44*10^-5;         % Kinematic viscosity of oil
mu=0.004;              % Viscosity in Pascal seconds
kr=0.15;               % Precipitation rate constant
Va=400; % Paraffins molar volume
turbulent=true;
%False forces lamniar velocity profile independent of Reynolds number.
n=5; % Number of simulations
dr=R/nj;
dz=L/ni;
z=linspace(0,L,ni); % Vector for dimensions along the first axsis
r=linspace(0,R,nj); % Vector for dimensions along the second axsis

% %% *********Making contour plot of concentration and temperature **********
T=temperature_calc(ni,nj,R,L,Q,nu,Tw,Ti,alpha0,turbulent);
C=concentration_calc(ni,nj,R,L,Q,nu,Tw,Ti,T,kr,turbulent,mu,Va);

figure(1);
contour(z,r,T,190), xlabel('Distance from inlet [m]');
ylabel('Radial distance from pipe axis'),colorbar;
title('Temperature distribution [C]');

figure(2);
contour(z,r,C,190), xlabel('Distance from inlet [m]');
ylabel('Radial distance from pipe axis[m]'),colorbar;
```

```
title('Concentration distribution [kg/m^3]');
% Script continues on next page.

% %% ****************Plotting Sherwood number against kr*********************

kr= [0.02 0.05 0.10 0.15 0.2]; % Vector with the differen kr-values
% we want to investigate, the number must not exceed number of ...
    simulations, n.

Sh=ones(n,ni); % A matrix for the calculated Sherwood numbers we want to plot
for k=1:n % Loop to produce Sherwood versus length for different kr's
    C=concentration_calc(ni,nj,R,L,Q,nu,Tw,Ti,T,kr(k),turbulent,mu,Va);
    % Producing a new C-matrix. Computational expensive.
    for i=1:ni
      dcdr=(C(nj,i)-C(nj-1,i))/dr; %dc/dr at the wall
      Sh(k,i)=-2*nj*dr*dcdr/(C(1,i)-C(nj,i)); % Sherwood number
    end
end

% Plotting the different Sherwood numbers versus the length
% Hardcoded for 5 parts
plot(z,Sh(1,:),z,Sh(2,:),z,Sh(3,:),z,Sh(4,:),z,Sh(5,:));
legend('kr=0.02','kr=0.05','kr=0.10','kr=0.15','kr=0.20');
xlabel('Distance from inlet [m]'), ylabel('Sherwood number');

% %% ******** Plotting concentration profiles in the boundary layer**********
n=5; % Number concentration profiles to simulate
kr= [0.02 0.05 0.10 0.15 0.2]; % Vector with the differen kr-values
% we want to investigate, the number must not exceed number of ...
    simulations, n.

profile=zeros(50,n);  % Matrix to store the concentration profile values in.
for k=1:n % Loop to produce concentration profiles for different kr's
    C=concentration_calc(ni,nj,R,L,Q,nu,Tw,Ti,T,kr(k),turbulent,mu,Va);
    for j=1:nj*0.9
        profile(:,k)=C((nj-49):nj,15);% Hardcoded for 50 data points.
    end
end

r=linspace(0.005955,R,50)'; % Making dimensions to the first axsis.
plot(r,profile(:,1),r,profile(:,2),r,profile(:,3),r,profile(:,4),r,profile(:,5));
xlabel('Radial distance [m]'), ylabel('Concentration [kg/m^3]');
legend('kr=0.02','kr=0.05','kr=0.10','kr=0.15','kr=0.20');
```